

# Forecasting vegetation condition for drought early warning systems in pastoral communities in Kenya

Adam B. Barrett<sup>a,b</sup>, Steven Duivenvoorden<sup>a,c</sup>, Edward Salakpi<sup>a</sup>, James M. Muthoka<sup>d</sup>, Seb Oliver<sup>a,c</sup> and Pedram Rowhani<sup>d\*</sup>

<sup>a</sup> *The Data Intensive Science Centre, Department of Physics and Astronomy, University of Sussex, Brighton BN1 9QH, UK*

<sup>b</sup> *Sackler Centre for Consciousness Science, Department of Informatics, University of Sussex, Brighton BN1 9QJ, UK*

<sup>c</sup> *Astronomy Centre, Department of Physics and Astronomy, University of Sussex, Brighton BN1 9QH, UK*

<sup>d</sup> *School of Global Studies, Department of Geography, University of Sussex, Brighton, BN1 9QJ, UK*

\*Corresponding author: P.Rowhani@sussex.ac.uk

---

## Abstract

Live version, post 1st review, pre resubmission This is such an amazing paper.

Droughts are a recurring hazard in sub-Saharan Africa, that can wreak huge socioeconomic costs. Acting early based on alerts provided by early warning systems (EWS) can potentially provide substantial mitigation in terms of money and lives lost. However existing EWS tend only to monitor, rather than forecast, the environmental and socioeconomic indicators of drought, and hence are not always sufficiently timely to be effective in practice. Here we make a first attempt [is it really first?, Seb] at forecasting satellite-based indicators of vegetation condition that are commonly monitored. Specifically, we forecast the Normalized Difference Vegetation Index (NDVI) and the Vegetation Condition Index (VCI) over pastoral livelihood zones in Kenya as these are the common indicators used by the National Drought Management Authority (NDMA). Using data from MODIS and Landsat, we apply linear autoregression and Gaussian processes modeling methods and demonstrate accurate forecasting several weeks ahead. We explored predicting the drought alert marker used by NDMA

(3 month VCI< 35). Both of our models were able to predict this alert marker four weeks ahead with a hit rate of around 89% and a false alarm rate of around 4%, or 81% and 6% respectively six weeks ahead. The methods developed here can identify a deteriorating vegetation condition well in advance and thus help disaster risk managers act early to support vulnerable communities and limit the impact of a drought hazard.

*Keywords:* Landsat; MODIS; Gaussian Processes; Drought; NDVI; VCI

---

<sup>1</sup> **1. Introduction**

<sup>2</sup> Droughts are a major threat globally as they can cause substantial damage  
<sup>3</sup> to society, especially in regions that depend on rain-fed agriculture. They par-  
<sup>4</sup> ticularly impact food security by significantly reducing agricultural production  
<sup>5</sup> (Lesk et al., 2016) and raising food prices (Nelson et al., 2014; Brown and Kshir-  
<sup>6</sup> sagar, 2015), which often leads to increased levels of malnutrition, migration,  
<sup>7</sup> disease, and other health concerns (Piguet et al., 2011; Stanke et al., 2013).  
<sup>8</sup> Since 2000, there have been 319 drought events reported (EMDAT 2019), which  
<sup>9</sup> together have killed over 21,000 people and affected almost 1.4 billion others.  
<sup>10</sup> The majority of these events took place in sub-Saharan Africa where many  
<sup>11</sup> communities rely on predictable rainfall patterns for their livelihood.

<sup>12</sup> In East Africa, the main economic activity in the arid and semi-arid lands  
<sup>13</sup> (ASAL) is subsistence rain-fed agriculture, as well as livestock farming using  
<sup>14</sup> pastures and grasslands as the main source of fodder. The pastoral and agro-  
<sup>15</sup> pastoral communities who live in these drylands have dealt with rainfall vari-  
<sup>16</sup> ability and drought over centuries by developing extensive adaptation and mit-  
<sup>17</sup> igation strategies to reduce their vulnerability to these shocks (Nyong et al.,  
<sup>18</sup> 2007; Orindi et al., 2007). However, in recent years these communities have  
<sup>19</sup> seen their coping strategies compromised by population growth and land use  
<sup>20</sup> change (Galvin et al., 2001). Additionally, while there is some uncertainty in

21 the climate models (IPCC, Stocker et al., 2013), rainfall variability is expected  
22 to increase in the region (Tierney et al., 2015; Yang and Huntingford, 2018).  
23 These factors in combination will make it harder for indigenous knowledge sys-  
24 tems to deal with droughts, and exacerbate the problems created by droughts.  
25 Governments and donor agencies in the region have thus developed several tools  
26 and early warning systems (EWS) to mitigate the impact of droughts on pas-  
27 toralists.

28 Most EWS tend to monitor current key biophysical and socio-economic fac-  
29 tors to assess the possible exposure of vulnerable people to specific hazards.  
30 However, once the impacts are visible, it will be too late to mitigate the con-  
31 sequences (Kogan et al., 2013). [As a consequence, there is growing interest in](#)  
32 [moving toward a proactive humanitarian approach to disasters \[Coughlan de](#)  
33 [Perez et al. 2015; Lopez et al 2018; Wilkinson et al. 2018\]. Additionally, it is](#)  
34 [estimated that](#) being better prepared before a drought hits significantly reduces  
35 the costs and losses from these disasters (Venton et al., 2012). Hence, EWS now  
36 increasingly include expert knowledge and qualitative assessments of seasonal  
37 climate forecasts to assess the future development of food security, and define  
38 actions to mitigate possible losses (Coughlan de Perez et al., 2015; Tozier de la  
39 Poterie and Baudoin, 2015).

40 Within East Africa, the Famine Early Warning Systems Network (FEWS  
41 NET) monitors food security through data collection and a deep understanding  
42 of the livelihood patterns in the region. A team of experts and analysts will  
43 also look at seasonal climate forecast to estimate future food security outcomes  
44 using scenario development (FEWS-NET, 2018). In Kenya, the drought EWS  
45 operated by the National Drought Management Authority (NDMA) provides  
46 monthly bulletins assessing food security in the 23 ASAL regions [using current](#)  
47 environmental (rainfall, vegetation condition) and socio-economic (production,

48 access, and utilisation) factors. Based on these factors, the bulletins include a  
49 qualitative evaluation of food security outcomes in the months ahead. **Shouldn't**  
50 **the next sentence be in the discussion, not here, because we are not addressing**  
51 **consequences in this paper and also our premise is that the current EWS do not**  
52 **forecast at all [Seb]Agreed! we should have whole paragraph on using forecasts**  
53 **and moving from hydro to impact-based [Pedram].** However, EWS should move  
54 from forecasting hydro-meteorological events toward estimating the expected  
55 consequences of hazards, i.e. impact-based forecasting, to identify more effective  
56 early action protocols (WMO, 2015; Sai et al., 2018).

57 Pastoralists strongly rely on forage availability to keep their livestock. **Ex-**  
58 **isting EWS provide information on pasture condition through the use of vege-**  
59 **tation indices that are derived from satellite-based Earth observation,** such as  
60 the Normalized Difference Vegetation Index (NDVI) and the Vegetation Con-  
61 dition Index (VCI, Kogan, 1995; Klisch and Atzberger, 2016; Rulinda et al.,  
62 2011; Rojas et al., 2011). These products are commonly used as drought indi-  
63 cators as they provide timely and regular assessment of vegetation health over  
64 large spatial areas. **Forecasts of these indicators within EWS** would allow lo-  
65 cal and national stakeholders **be better prepared and act early to support the**  
66 pastoralists in times of drought. Recent studies have highlighted the potential  
67 of satellite-based Earth observation data to forecast agricultural productivity  
68 (Zambrano et al., 2018) and seasonal forage availability (Vrieling et al., 2016).

69 The main goal of this paper is to explore methods to forecast (**up to six weeks**  
70 **ahead**) the vegetation indices that are commonly used in the pastoral areas of  
71 Kenya to monitor droughts. We specifically aim to estimate the potential to  
72 forecast NDVI **anomaly?** and the 3-month VCI (VCI3M), as used by the NDMA  
73 in their monthly bulletins. **Their drought early warning system includes clear**  
74 **thresholds of VCI3M which are used to classify drought severity in the ASAL**

75 regions of Kenya [Klisch et al]. Here, we extract the indices from data derived  
76 from the Landsat mission (every 16 days at 30 m resolution) and the MODerate  
77 resolution Imaging Spectroradiometer (MODIS - daily data at 500 m resolution).

78 Machine-learning techniques offer a data-driven, empirical route to these  
79 forecasts. Many different data inputs could be used to forecast these vegetation  
80 indices (e.g. precipitation and precipitation forecasts. However, perhaps the  
81 most simple is to use the past history of the indices themselves. This has the  
82 practical benefits of readily available data over large areas. It is also likely  
83 to work as these indices are subject to plant growth and climate cycles giving  
84 periodic behaviour on large temporal scales that can be empirically modelled  
85 while external perturbations, such as water availability, have persistent impact  
86 providing correlations on short temporal scales. The existing EWS itself implies  
87 that the indices have forecasting power as moderately low indexes are labelled  
88 “alert” implying they might precede lower “alarm” levels. something about  
89 the Boku paper herei do not understand this paragraph

90 The machine-learning techniques we attempt are Gaussian Process regression  
91 (GP, Rasmussen and Williams, 2006), and linear autoregressive (AR) modelling  
92 (e.g. Hamilton, 1994). GP regression uses kernel-based non-parametric  
93 Bayesian inference on the structure of correlations between observations, and  
94 is widely applied to classification, interpolation, change detection and forecasting  
95 problems (Brahim-Belhouari and Vesin, 2001; Chandola and Vatsavai, 2011;  
96 Camps-Valls et al., 2016; Upreti et al., 2019). For an overview on the principles  
97 of GPs, and how they have previously been applied throughout remote sensing,  
98 see Camps-Valls et al. (2016). Linear AR is the regression of future observations  
99 on past observations, assuming a linear dependence. This has previously been  
100 performed on monthly (i.e. temporally more sparse) NDVI data, see for example  
101 Asoka and Mishra (2015) and Papagiannopoulou et al. (2017), with mixed

102 results in terms of forecasting potential ( $R^2$ -scores between 0 and 0.4 at a lead  
103 time of one month).

104 I think this introduction needs something to end on that leads into the paper  
105 better

106 **2. Study area and our chosen drought indicator**

107 In Kenya, the livestock sector accounts for 13% of the national GDP and 43%  
108 of its agricultural GDP. Livestock farming mainly occurs in the ASAL which  
109 cover about 80% of the country (UNDP, 2013; FAO, 2014). In these regions,  
110 the pastoral communities rely on pastures and grasslands as the main source of  
111 fodder (Behnke and Muthami, 2011). Thus, providing information on pasture  
112 productivity to these communities is key in times of drought.

113 Following several periods of intense drought, the government in Kenya es-  
114 tablished the NDMA in 2016, to set up and operate a drought early warning  
115 system (DEWS), as well as to establish drought preparedness strategies and  
116 contingency plans (GoK)  
this should be reference - I will have to dig it out. And  
remove the previous acronym DEWS as it is not used much.

118 One key biophysical indicator used by the NDMA drought phase classifica-  
119 tion is the VCI (Klisch and Atzberger, 2016). The VCI, which expresses the  
120 NDVI as a fraction of its limiting range for a given pixel [Kogan et al 1995, (see  
121 Equation 1)], is one of a number of satellite-based indicators that have been  
122 developed to detect and monitor drought [Zargar et al. 2011]. While there is  
123 little agreement between VCI and precipitation-based meteorological drought  
124 indicators [Quiring and Ganesh 2010, Bhuiyan et al 2006], it is strongly linked  
125 to agricultural production and widely used to identify drought onset, intensity,  
126 duration, and impact [Jiao et al 2016, Klisch and Atzberger]. The NDMA uses  
127 the 3-month averaged VCI (VCI3M) in its operational EWS. Once the VCI3M

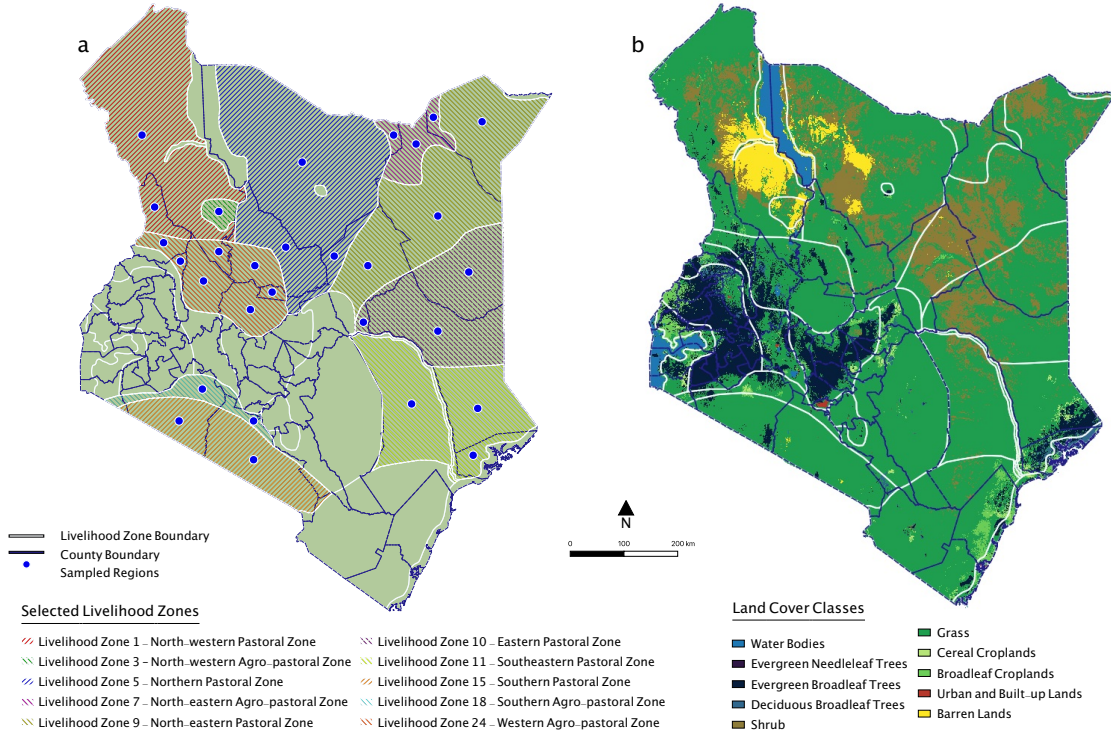


Figure 1: Maps of Kenya showing (a) the livelihood zones from which pixels were sampled for analysis, and (b) land cover classification (according to the MODIS MCD12Q1 data). Analyses were performed for 29 regions, defined by pastoral livelihood zone and county intersections. **is the next sentence needed?** For the MODIS data only those pixels identified as being from grassland are used.

128 goes below 35, the NDMA triggers a rapid food security assessment and has  
 129 access to the National Drought Contingency Fund in order to implement its  
 130 preparedness strategies and contingency plans [GoK 2013].

131 NDMA reports VCI3M at county level as well as over the different livelihood  
 132 zones within the county (FEWS NET 2011). This study focused on the 10  
 133 (agro)-pastoral livelihood zones (see Fig 1), which cross 15 counties. The names  
 134 of the 29 livelihood zone county intersections can be found in Appendix D.1.

135     **3. Data preprocessing**

136     This research is based on two satellite-based Earth observation datasets,  
137     Landsat and MODIS. A comparison between them, and justification of data  
138     selection can be found in Appendix A. We economise on data processing by  
139     performing the data preprocessing on a random subsample of the pixels within  
140     each of the 29 pastoral livelihood zone and county intersections of interest (Fig.  
141     1).

142     A summary of the entire work from data preparation to forecasting drought  
143     can be seen in Figure 2.

144     *3.1. Landsat*

145     Landsat-5, 7 and 8 (Roy et al., 2014) red and near infrared (NIR) surface  
146     reflectances and quality assessment (QA) data over the 10 pastoral livelihood  
147     zones of Kenya, from January 1st, 2000 to February 1st, 2019, were obtained  
148     using the United States Geological Survey (USGS) EarthExplorer. Specifically,  
149     data were drawn from the Level-1 Precision Terrain (L1TP) processed dataset,  
150     which has well-characterized radiometry and is inter-calibrated across the differ-  
151     ent Landsat sensors. The spatial resolution of these data is 30m and the repeat  
152     interval is 16 days. Using the QA data, observations classified as clear were  
153     kept. Pixels with fewer than half of the observations over the full time period  
154     were discarded (with a few exceptions, see Table D.8). The surface reflectances  
155     were combined to obtain NDVI<sup>1</sup> from which we derived the NDVI anomaly and  
156     VCI (see Eq. 1).

157     The temporal aggregation and gap-filling on the Landsat data was done using  
158     Gaussian Process (GP) modelling; see 4.1. For a given pixel, the GP modelling  
159     took raw data as input, fit a temporal correlation structure to the data, and

---

<sup>1</sup>NDVI = (NIR – Red)/(NIR + Red)

160 used this to output a time series of expected NDVI values, with observations  
161 provided every Saturday over the studied time period. Two versions of GP  
162 gap-filling were carried out, which we refer to as forecast mode and non-forecast  
163 mode. For the non-forecast mode, the full time series from the given pixel were  
164 used to train the GP. The non-forecasting mode was used as the “ground truth”  
165 to test forecasts against. The forecast mode, by contrast, only used data up to  
166 a certain date, whichever date a forecast was being attempted from - since when  
167 doing forecasting with a near real-time data stream, one does not have access  
168 to future data.

169 1 000 random pixels were selected for processing.

170 *3.2. MODIS*

171 The NDVI was also derived from the surface reflectances obtained from  
172 the daily, 500-meter resolution MODIS Terra/Aqua Nadir BRDF-Adjusted Re-  
173 flectance product (MCD43A4,v006; Schaaf and Wang, 2015). Data from Febru-  
174 ary 22nd, 2000 up to February 1st, 2019 were acquired via the NASA Land  
175 Processes Distributed Active Archive Center.

176 there is no info on QA for MODIS, EDDIE can you please add a sentence,  
177 something like, Observations of poor quality, either due to cloud cover or unre-  
178 liable BRDF corrections, were removed using the quality flags.

179 Weekly NDVI composites were obtained by taking the mean of all available  
180 data over a 7-day time period. Gaps in the weekly timeseries (i.e., if all seven  
181 observations were of poor quality) were then filled using quadratic interpolation.  
182 (Gaps greater than 6 weeks were left unfilled, see Appendix B.1 for more de-  
183 tail.) The gap-filled timeseries were then smoothed using Savitzky-Golay (SG,  
184 Savitzky and Golay, 1964) to filter high-frequency measurement noise. The  
185 smoothing involved fitting, for each pixel, a polynomial to a window centred  
186 on the observation, and then replacing that observation with the output of the

187 polynomial fit. To determine the optimal window length, the polynomial order  
188 was set to 2 and different windows lengths were tested as done by Chen et al.  
189 (2004); Kandasamy et al. (2013). As a result, the length of the window was set  
190 to 7 time-steps (weeks) with a polynomial of order 2 (i.e. quadratic function) as  
191 it filtered out noise without smoothing out too much.

192 100 random grassland pixels, as identified by the MODIS land cover classi-  
193 fication maps (MCD12Q1,v006), were selected for processing.

#### 194 4. Methods

For both datasets, the weekly NDVI timeseries of the sampled pixels were converted to NDVI anomalies (i.e., the mean-subtracted NDVI) and VCI, which at time point  $i$  is being defined as:

$$VCI_i = 100 \times \frac{NDVI_i - NDVI_{min,i}}{NDVI_{max,i} - NDVI_{min,i}}, \quad (1)$$

195 where  $NDVI_{min,i}$  and  $NDVI_{max,i}$  are the minimum and maximum values for the  
196 NDVI of the pixel in the given week over all years covered by the data. With  
197 Landsat data, the mean, maximum and minimum value for the NDVI for each  
198 week of the year was computed using the non-forecast mode GP interpolated  
199 time series. Then forecast mode and non-forecast mode versions of each index  
200 were created. Next, we calculated VCI3M as the mean VCI across the 12 weeks  
201 leading up to the given observation time point.

202 The data within each livelihood zone and county intersection was aggregated  
203 taking the mean of the sampled pixels at each time step. Thus forecasting was  
204 applied on a single time series for each region (see Fig. 3 for an example time  
205 series). With the MODIS data, since large gaps were unfilled, whenever there  
206 were fewer than 25 individual datum from a particular region at a given time,  
207 it was decided that there should be no datum in the aggregate time series (i.e.,

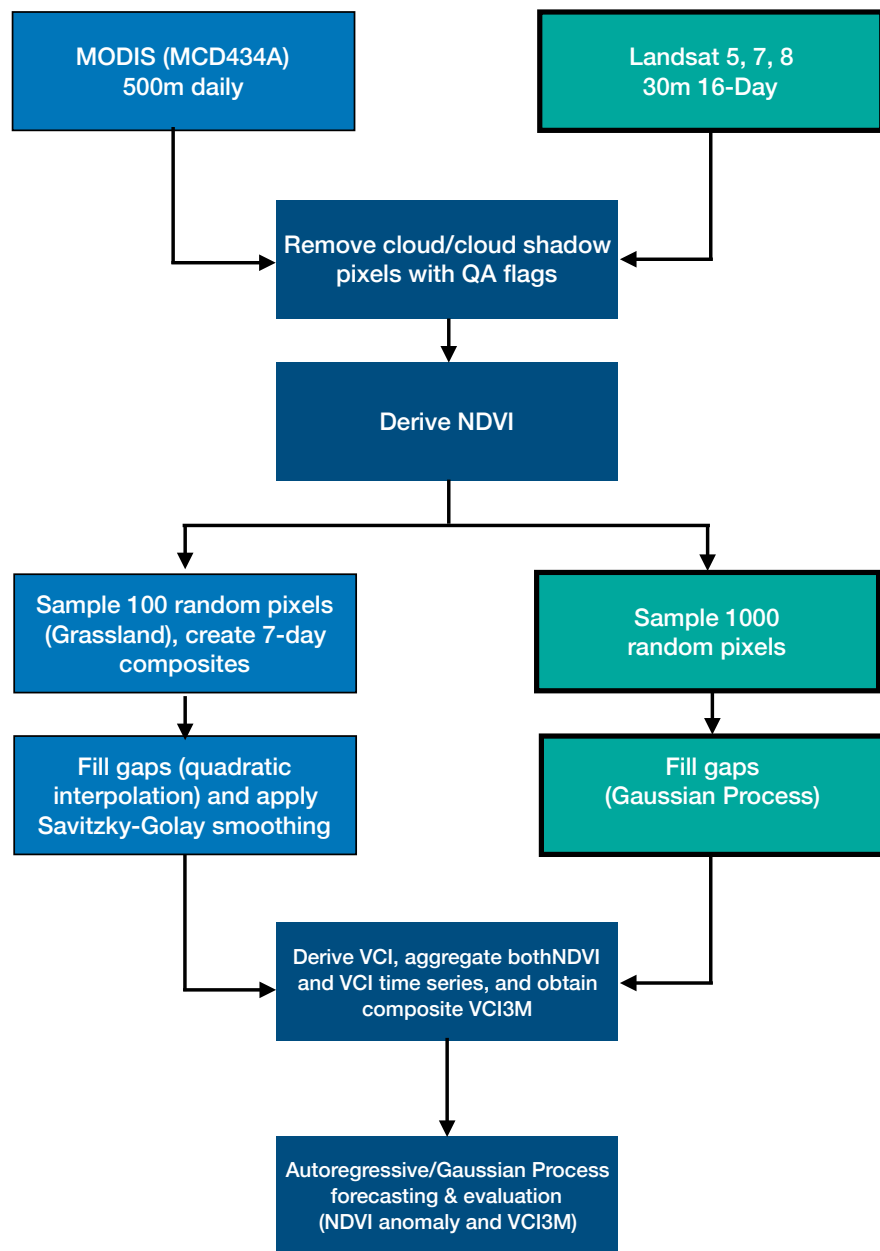


Figure 2: A Flow chart of the data processing and analysis

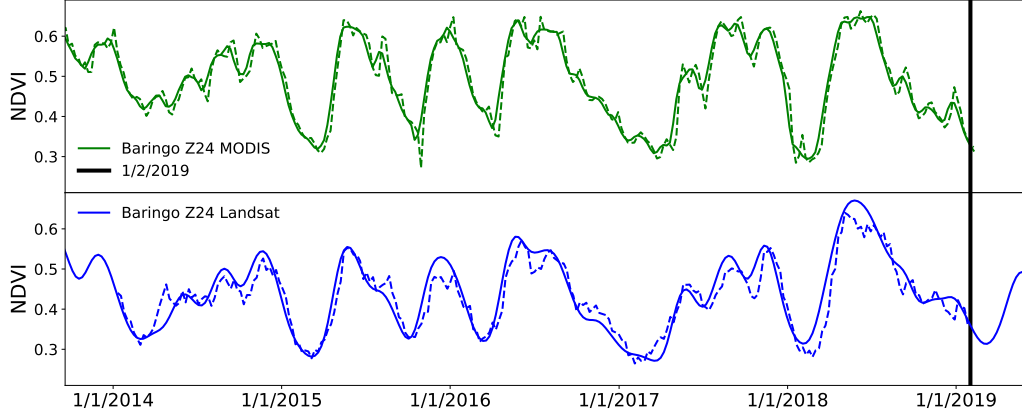


Figure 3: Aggregated NDVI time series from the intersection of Baringo county and livelihood zone 24. The top panel shows MODIS data, and the bottom panel shows Landsat data (solid lines), processed using the methods described in the text. The dotted lines in each panel show forecasting at a lead time of 2 weeks, using the AR method on the MODIS data, and the GP method on the Landsat data.

208 there should be a gap in the timeseries). It should be noted that VCI3M is the  
 209 mean of the most recent 12 weeks of VCI observations. Hence, if some of these  
 210 were missing, the mean was taken over just the ones that were present. If the  
 211 current observation was not present, a gap was placed in the VCI3M time series.  
 212 **THIS IS INCONSTANT WITH THE PREVIOUS PARA WHICH IMPLIES**  
 213 **THAT THE VCI3M CALCULATION IS DONE \*BEFORE\* AGGREGATION**

214 *4.1. Forecasting*

215 Forecasts of the various indices were calculated using two separate methods,  
 216 Gaussian Process regression (GP) and linear autoregressive (AR) modelling.

A Gaussian Process is a probabilistic model defined as a collection of random variables for which any finite subset has a joint Gaussian distribution (Ras-

mussen and Williams, 2006). Formally, for an output  $y$  and inputs  $\mathbf{x}$ :

$$f(\mathbf{x}) \sim \mathcal{GP}(m(\mathbf{x}), k(\mathbf{x}, \mathbf{x}')), \quad (2)$$

$$y_i = f(\mathbf{x}_i) + \sigma_r, \quad (3)$$

where the mean function  $m(\mathbf{x})$  represents the expectation  $E[f(\mathbf{x})]$  and the kernel function  $k(\mathbf{x}, \mathbf{x}')$  defines the covariances  $\text{cov}(f(\mathbf{x}), f(\mathbf{x}'))$ , which specifies how similar outputs  $f(x)$  and  $f(x')$  are. The sample drawn from  $f(\mathbf{x})$  at locations  $\mathbf{x}_{n=1}^N$  follow a joint multivariate Gaussian distribution with covariance matrix determined by the kernel function. Here, the  $\mathbf{x}_i$  is the dates,  $t_i$ , of the observations (i.e. one dimensional), and  $y_i$  is the NDVI at date [can we check we've been consistent about the use "date", "time", "time-step" etc.]  $t_i$ , subject to measurement error,  $\sigma_r$ . To interpolate, the existing data were used to fit the mean,  $m$ , and the kernel,  $k$ , and then the GP provided an estimate of the probability distribution for the missing or future data.

### SEB HERE

The mean,  $m(t)$ , was modelled as a constant over the whole time series. To determine the kernel, compositional Kernel Search (Duvenaud et al., 2013) was used to determine the best kernel combination, by calculating the maximum evidence<sup>2</sup> (marginal likelihood) for any product or sum of two common kernel combinations (Linear, Radial Basis Function, Periodic, Rational Quadratic and Matern). The kernel with the highest evidence for the Landsat NDVI time series was the Radial Basis Function (RBF) in addition to the Periodic kernel

---

<sup>2</sup>In practice the evidence lower bound (ELBO) was used instead of the evidence ( $p_\sigma$ ) with  $\log(p_\sigma) \geq \text{ELBO}$

$(k_{RBF} + k_P)$ , where the period  $p$  was set to one year:

$$k_{RBF}(t, t') = \sigma_{RBF}^2 \exp\left(-0.5 \frac{|t - t'|^2}{l_{RBF}^2}\right), \quad (4)$$

$$k_P(t, t') = \sigma_P^2 \exp\left(-2 \frac{\sin^2(\pi|t - t'|/p)}{l_P^2}\right). \quad (5)$$

228 This GP contains 5 parameters to be fit ( $\sigma_r, \sigma_{RBF}, l_{RBF}, \sigma_P, l_P$ ), which were  
 229 learned using Stochastic Variational Inference (SVI). The code was written using  
 230 the Deep Universal Probabilistic Programming language from **Pyro**, which is  
 231 written in **Python** and supported by **PyTorch**.

AR forecasting was performed with the following model-fitting and extrapolation method. For forecasting  $n$  weeks ahead, the following model was fit:

$$X_{t+n} = \sum_{i=0}^{p-1} a_i X_{t-i} + \epsilon_t, \quad (6)$$

232 where  $X$  is NDVI anomaly (or VCI3M with mean removed) **doesn't this make**  
 233 **it an anomaly of an anomaly? and are you forecasting VCI3M anomaly?**, sub-  
 234 scripts denote the observation (week),  $a_i$  are model parameters,  $\epsilon_t$  are the resid-  
 235 uals (i.e. the errors), and  $p$  is the model order. Fitting the model to a segment of  
 236 data involved finding the model parameters that gave the minimum sum-square  
 237 error, i.e. led to residuals with the minimum variance. To make a forecast, the  
 238 model was fit using the most recent  $T$  consecutive observations, and then used  
 239 to predict the observation  $n$  weeks after the most recent observation. This fore-  
 240 casting method was carried out along the entire available time series, fitting a  
 241 distinct model to each segment of length  $T$ . A search for optimal model orders  
 242 and training segment lengths found that forecast quality, as measured by root  
 243 mean square error (RMSE), plateaued at  $T = 200$  and  $p = 3$ .

Table 1: TO DO: STEVEN/EDWARD FILL THIS OUT FOR GP/LANDSAT.  
change the x axis to months Performance statistics of NDVI anomaly and VCI3m forecasting.

	Landsat GP			MODIS AR		
	2 weeks	4 weeks	6 weeks	2 weeks	4 weeks	6 weeks
<b>NDVI anomaly:</b>						
$R^2$ -score	0.66	0.42	0.21	0.85	0.55	0.33
RMSE	0.031	0.04	0.047	0.025	0.043	0.053
slope	1.14	1.25	1.38	0.99	0.99	0.97
intercept	0.006	0.009	0.011	-0.00	-0.00	-0.00
<b>VCI3M:</b>						
$R^2$ -score	0.99	0.95	0.85	0.99	0.96	0.88
RMSE	1.94	4.41	7.286	1.8	4.3	7.0
slope	1.024	1.059	1.11	1.00	1.00	1.00
intercept	-0.62	-1.55	-2.95	-0.0	-0.1	-0.0

<sup>244</sup> 4.2. Metrics for assessing forecasts

Several metrics were used to assess the performance of the forecast methods tested on the data. In addition to RMSE, the  $R^2$ -score and the percentage of standard deviation remaining,  $S$ , were used. These are given by:

$$R^2\text{-score} = 1 - \frac{\sum_i (y_i - f_i)^2}{\sum_i (y_i - \bar{y})^2}, \quad (7)$$

$$S = 100 \times \frac{\sqrt{\sum_i (y_i - f_i)^2}}{\sqrt{\sum_i (y_i - \bar{y})^2}}, \quad (8)$$

<sup>245</sup> where the  $y_i$  are the true data, and the  $f_i$  are the forecasts. Note that  $S \equiv$   
<sup>246</sup>  $100 \times \sqrt{1 - R^2\text{-score}}$ . To test for bias, linear regression of actual index on  
<sup>247</sup> forecast index was performed, and slope and intercept computed. Finally, re-  
<sup>248</sup> ceiver operating characteristic (ROC) curves were constructed for forecast-based  
<sup>249</sup> drought-alert detection.

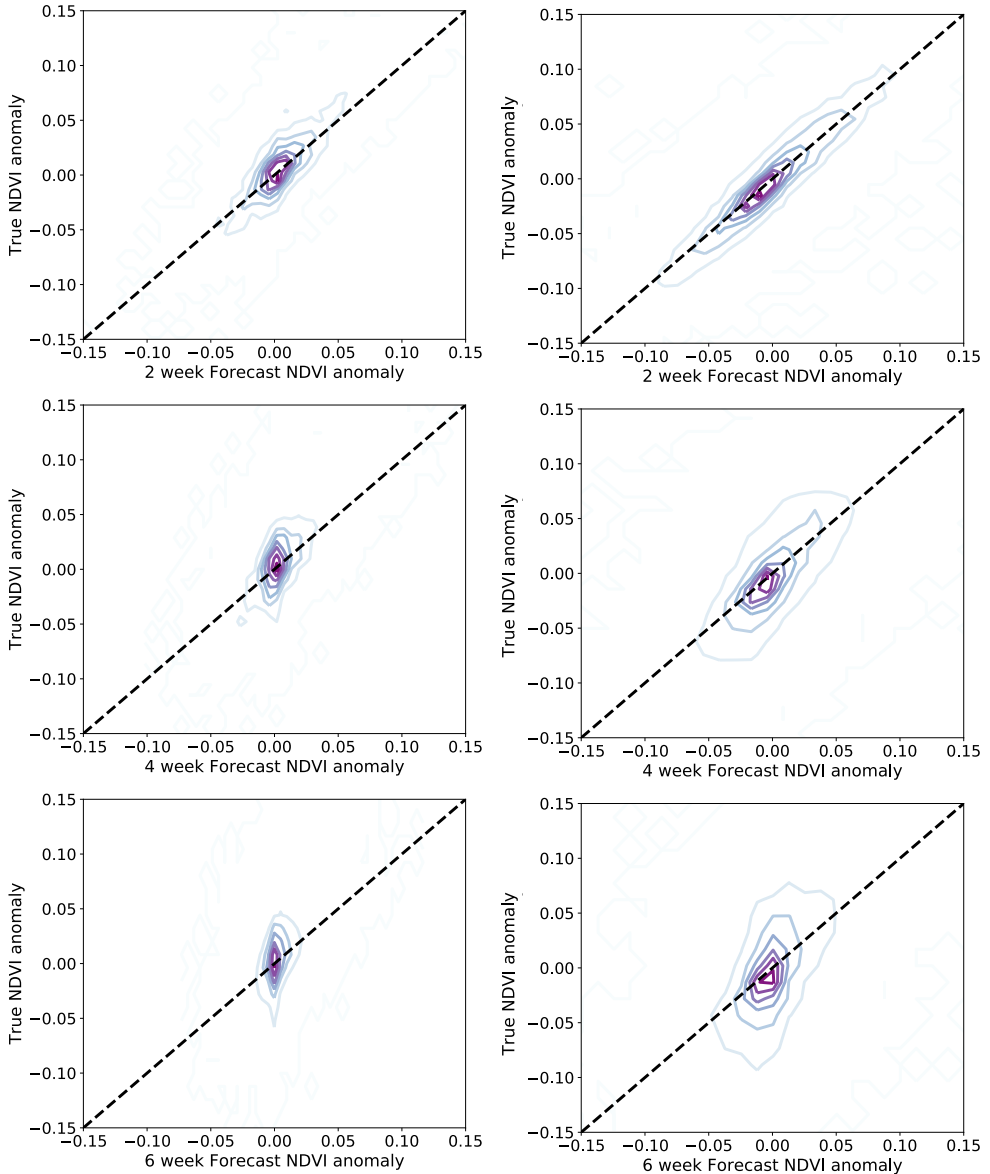


Figure 4: TO DO: EDWARD, REFORMAT SO Y AXIS LABEL IS VISIBLE. ALSO EACH PANEL NEEDS AN IDENTIFIER a, b, c, d, e, f. Contour plots of NDVI anomaly against our two, four and six weeks NDVI anomaly forecast. (a,c,e) show our forecast performance for the GP method on Landsat data, and (b,d,f) show the forecast performance for the AR method on MODIS data, across the 19 regions for which a forecast is possible more than 50% of the time. what does this last bit mean

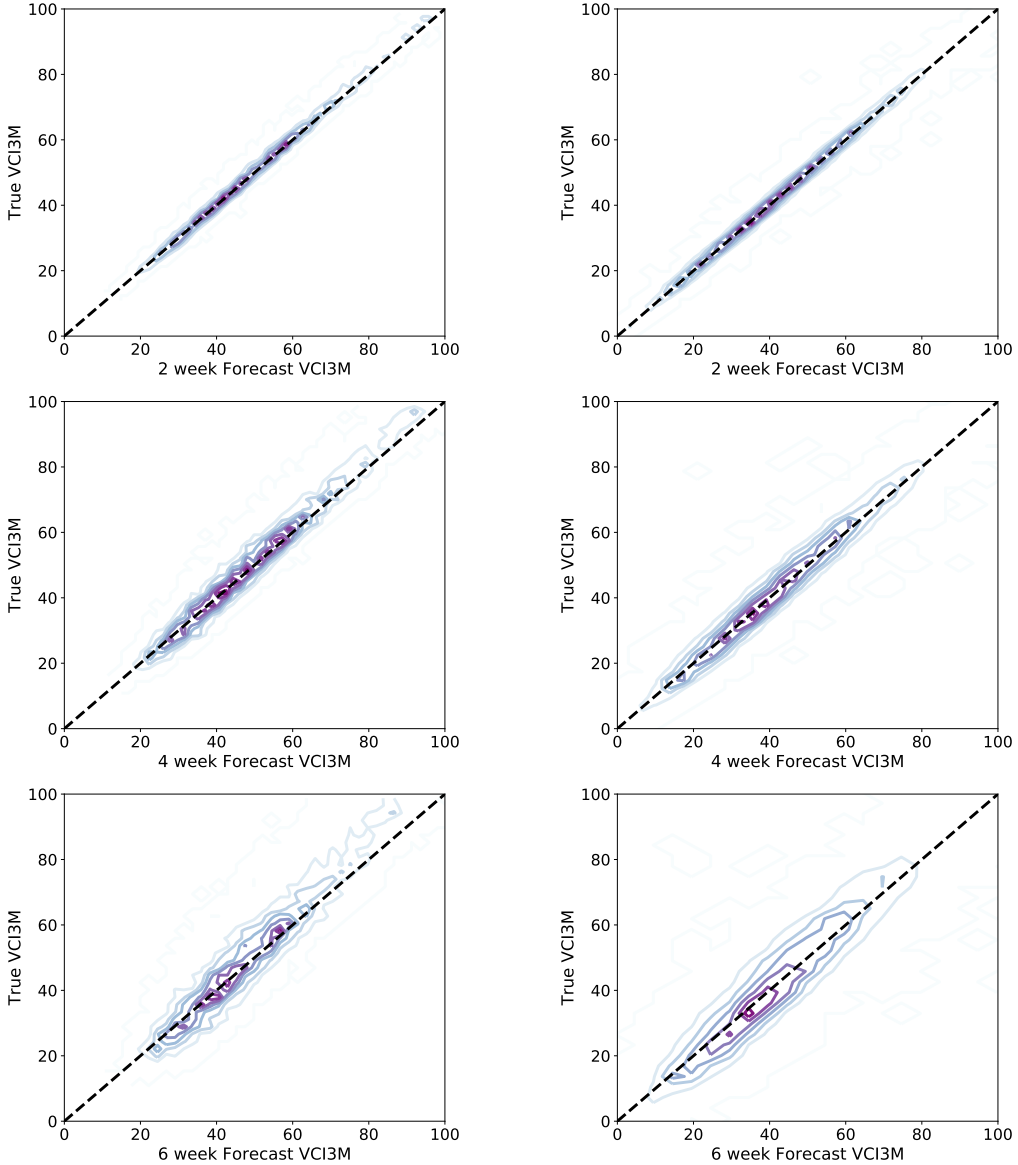


Figure 5: SAME AS BEFORE! Contour plots of VCI3M against our two, four and six weeks VCI3m forecast. (a,c,e) show our forecast performance for the GP method on Landsat data, and (b,d,f) show the forecast performance for the AR method on MODIS data, across the 19 regions for which a forecast is possible more than 50% of the time.

250    **5. Results**

251    *5.1. Forecast values compared with true values*

252    The GP and AR forecasting methods were applied, on each of the two  
253    datasets, to regional aggregate NDVI and VCI3M time series. We focus on  
254    performance results of GP forecasting on Landsat data and AR forecasting on  
255    MODIS data since these two combinations of data and forecasting method per-  
256    formed the best (as measured by  $R^2$ -score, see Appendix D.1). Contour plots  
257    of forecast against actual data for two, four and six week forecasts are shown  
258    in Fig. 4 for NDVI anomaly, and Fig. ?? figure number! for VCI3M. Table  
259    1 shows the  $R^2$ -scores, RMSE, slope and intercept from each of these plots,  
260    and demonstrates that there is substantial forecast skill from each method at  
261    each lead time ( $R^2$ -scores are substantial), and that the forecasts are unbiased  
262    (slopes are all approximately 1, and intercepts approximately 0). The much  
263    higher  $R^2$ -scores for VCI3M compared to NDVI anomaly is explained by the  
264    fact that VCI3M is a 12 week aggregate, and hence its (near) future is actually  
265    derived from both past and future NDVI values. but this is not exactly how we  
266    did it. can we please discuss this together?

267    Due to the presence of non-interpolated gaps in the MODIS time series,  
268    there were weeks when a forecast assessment was not carried out on these data,  
269    see Section Appendix B.1 in the Supplementary Material for details. For 15 of  
270    the regions, a 4 week forecast could be made on more than 90 percent of weeks;  
271    however, for some of the more cloudy/wet regions, a forecast could rarely be  
272    made, see Table D.10.

273    To check if forecast skill depended on the true vegetation condition, the RMS  
274    error was also computed separately for each of the five categories on the NDMA  
275    drought scale Klisch and Atzberger. The results are shown in Table 2, where  
276    it can be seen that RMS error tended to be lower when there was a state of

Table 2: RMS error in VCI3M forecast, for the true vegetation condition belonging to the different categories of drought, at lead times of 2, 4 and 6 weeks. (The bottom category, extreme drought, did not occur according to the Landsat data.)

Drought category	Landsat GP			MODIS AR		
	2 weeks	4 weeks	6 weeks	2 weeks	4 weeks	6 weeks
Wet, VCI3M>50	2.2	5.3	9.0	2.2	4.8	7.5
Normal, 35<VCI3M<50	1.7	3.4	5.0	1.6	4.0	6.5
Moderate drought, 20<VCI3M<35	1.5	3.2	5.0	1.5	3.7	5.7
Severe drought, 10<VCI3M<20	1.1	2.5	5.5	1.4	3.3	5.4
Extreme drought, VCI3M<10				1.1	2.9	4.8

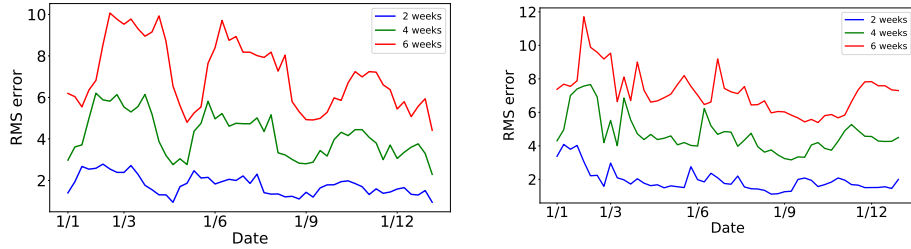


Figure 6: TO DO: STEVEN/EDWARD REPLACE LEFT HAND PLOTS WITH THE CORRESPONDING PLOTS FROM LANDSAT/GP. RMS error of VCI3M forecast for each week of the year. (Left) GP forecasting on Landsat data. (Right) AR forecasting on MODIS data.

drought than when the vegetation condition was normal.

To check if forecast skill depended on the time of year, RMS error of VCI3M forecast was plotted against the week of the year, see Fig. 6. The plot shows that the seasonal differences in RMS error are not substantial on the scale on which VCI3M varies, although RMS error was generally somewhat elevated for some of the January/February dry season.

### 5.2. Drought event forecast: ROC curves

To assess the usefulness of the AR and GP methods for drought forecasting, we tested their ability to detect specific drought events, as defined by the NDMA's alert threshold (VCI3M<35, Klisch and Atzberger, 2016). ROC curves were plotted for the detection of VCI3M<35 at lead times of two, four and six weeks (Fig. 7). These curves show the probability of predicting a state of

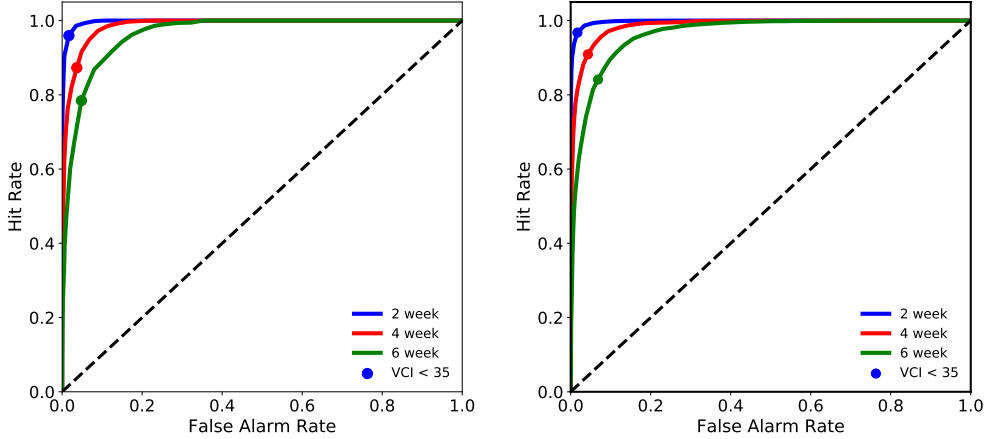


Figure 7: (Left) ROC curve for drought detection ( $VCI3M < 35$ ) for lead times of 2, 4 and 6 weeks using the GP method. (Right) ROC curve for drought detection using the AR method. The curves are plotted from applying different thresholds to convert the continuous forecast into a binary forecast of drought or no drought, see text for details. The shaded circles show the point obtained from forecasting drought when the predicted  $VCI3M < 35$ . The area under the curve is 1.0, 0.98, 0.96 (GP, left) and 1.0, 0.99 and 0.96 (AR, right) for lead times of two, four and six weeks, respectively.

drought ( $VCI3M < 35$ ) when there will be a state of drought, i.e. hit rate, against the probability of predicting drought when there will not be drought, i.e. false alarm rate, for varying binarisation thresholds on the forecast. These curves give an indication that one can **reliably** forecast droughts with these methods even as far as six weeks ahead.

The ROC curve performance is not highly dependent on the region (see Table 3). Even for the wetter Eastern regions, for which observations are sparser due to cloud cover, the hit and false alarm rates only differ by 1 to 2 percentage points compared with those computed across all regions. **Further, ROC curves for predicting the NDMA drought categories of severe ( $10 < VCI3M < 20$ ) or extreme ( $VCI < 10$ ) drought look similar to those for detecting  $VCI3m < 35$ , see Fig. D.12.** Together, these results demonstrate that there is a **strong** potential for drought forecasting **using these commonly-used indicators**, and we encourage a future

Table 3: False alarm rate and hit rate (respectively, in percent) for different regions in Kenya based on forecasting drought if the predicted VCI3M is less than 35.

Regions	Landsat GP			MODIS AR		
	2 weeks	4 weeks	6 weeks	2 weeks	4 weeks	6 weeks
All	2% 96%	4% 87%	5% 78%	2% 97%	4% 91%	7% 84%
Z24	2% 99%	4% 91%	5% 82%	2% 98%	5% 94%	8% 88%
North (Z1,3 and 5)	1% 97%	2% 88%	3% 76%	2% 98%	6% 93%	11% 87%
East (Z7, 9, 10 and 11)	3% 94%	5% 85%	6% 77%	3% 97%	6% 91%	10% 85%
South (Z15 and 18)	1% 96%	3% 88%	4% 77%	2% 98%	6% 94%	11% 90%

302 cost-benefit analysis of applying such a forecast in practice.

## 303 6. Discussion and Conclusion

304 This paper highlights the potential of two separate methods for drought fore-  
 305 casting in pastoral regions of Kenya. The linear autoregression models applied  
 306 to MODIS achieved an  $R^2$ -score of 0.58 for NDVI anomaly at a lead time of  
 307 4 weeks, and an  $R^2$ -score of 0.95 for the VCI3M, the three-month vegetation  
 308 condition index used within the drought early warning system developed by the  
 309 National Drought Management Authority. The Gaussian Processes method was  
 310 applied to Landsat and achieved an  $R^2$ -score of 0.36 for NDVI anomaly at a lead  
 311 time of 4 weeks, and an  $R^2$ -score of 0.94 for the VCI3M. In comparison to the  
 312 results published by Adede et al. (2019), the  $R^2$ -scores for VCI3M 4 weeks ahead  
 313 by both our methods were better than the 1-month VCI3M forecast ( $R^2$ -scores  
 314 of 0.78) with their Artificial Neural Network(ANN) approach . Importantly,  
 315 both methods showed high sensitivity and specificity for prediction of VCI val-  
 316 ues indicative of drought, at lead times of 2, 4 and 6 weeks (see Fig. 7). We  
 317 have presented results at the level of livelihood zone and county intersections,  
 318 however both methods can be applied at any suitable spatial unit (e.g., grazing  
 319 units) due to the high spatial resolution of both satellite datasets.

320 Both methods constitute novel analyses of vegetation index time series. To  
 321 our knowledge, this is the first time that the GP method for NDVI forecasting

322 has been applied to large amounts of real data and used for gap-filling. We  
323 have shown that GPs are a very useful addition to other methods for both these  
324 purposes. Similarly, linear AR of NDVI, or of Granger causality of various  
325 variables to NDVI, has not previously been explored at a temporal resolution  
326 as fine as 1 week. That such substantial  $R^2$ -scores can be achieved for NDVI  
327 anomaly at a lead-time of several weeks just by using the past few observations  
328 of NDVI anomaly in a linear AR model is a novel finding. Furthermore we  
329 moved beyond fitting a single model, and rather fit models to segments of data,  
330 repeatedly using refreshed models to forecast subsequent observations not used  
331 in the model fitting (i.e. we had separation of training and testing models).

332 Droughts have many adverse effects on pastoral and agro-pastoral commu-  
333 nities as they mainly rely on rainfall for food and fodder availability. In order  
334 to reduce drought-related damage and losses within these communities, local,  
335 national, and international stakeholders often decide to act on information pro-  
336 vided by EWS which may come too late (Kim and Guha-Sapir, 2012). Indeed,  
337 these systems tend to monitor current, rather than forecast future, environ-  
338 mental and socio-economic factors in a region, and sound the alarm when the  
339 situation is already critical. Some EWS now include a qualitative assessment  
340 of future rainfall. However, a meteorological or hydrological drought will not  
341 necessarily lead to agricultural damage (Bhuiyan et al., 2006). To mitigate the  
342 impacts on food security and nutrition, EWS need to focus on monitoring and  
343 forecasting the possible socio-economic impacts of future rainfall variability on  
344 agricultural drought (WMO, 2015). Additionally, acting ahead of a disaster in-  
345 stead of providing humanitarian assistance once a disaster hits can save money  
346 and lives (Venton et al., 2012). The methods developed in this study allow  
347 disaster risk managers to estimate vegetation condition to access resources and  
348 limit the impacts for pastoralist communities up to six weeks ahead. For exam-

<sup>349</sup> ple, in Kenya, the emergency funds that are linked to the VCI could be accessed  
<sup>350</sup> earlier to launch livestock destocking and vaccination campaigns. Future work  
<sup>351</sup> should focus on methods that forecast socio-economic drought indicators such  
<sup>352</sup> as livestock mortality, milk production, or food prices.

<sup>353</sup> Droughts are complex and hence inherently difficult to define and measure  
<sup>354</sup> (Mishra and Singh, 2010). A large number of satellite-based indicators have been  
<sup>355</sup> developed to identify meteorological, hydrological, and agricultural droughts  
<sup>356</sup> (Zargar et al., 2011; AghaKouchak et al., 2015) with each performing well in  
<sup>357</sup> space and time to a certain degree (Zhang et al., 2017). While its limitations  
<sup>358</sup> are known, the VCI used in this study has been introduced as one of the main  
<sup>359</sup> biophysical indicators in the drought early warning system operated by the  
<sup>360</sup> NDMA, with specific thresholds to identify different levels of drought throughout  
<sup>361</sup> the ASAL regions of Kenya (Klisch and Atzberger, 2016). In future, we suggest  
<sup>362</sup> that the performance of this indicator together with the thresholds used should  
<sup>363</sup> be linked to ground-based measurements over various agro-ecological zones.

<sup>364</sup> Droughts have devastating impacts on many people around the world. There  
<sup>365</sup> are increasing efforts to develop tools and identify actions to save lives and liveli-  
<sup>366</sup> hoods before these disasters strike. The methods developed in this study can  
<sup>367</sup> help policy makers, disaster risk managers and other key stakeholders to under-  
<sup>368</sup> stand up to six weeks in advance the state of vegetation in pastoral areas. This  
<sup>369</sup> will allow them to access resources and develop procedures before the impacts of  
<sup>370</sup> drought become visible to mitigate the adverse effects in these vulnerable com-  
<sup>371</sup> munities. To further strengthen EWS, future research needs to clearly identify  
<sup>372</sup> satellite-based indicators and thresholds of drought (which may vary in time  
<sup>373</sup> and space), to build a relation between observable indices and future impacts.  
<sup>374</sup> More work is also needed to understand how a hazard (e.g., reduced rainfall)  
<sup>375</sup> becomes a disaster (e.g., food insecurity) so that these events can be better

<sup>376</sup> forecasted.

<sup>377</sup> **Authors responsibilities**

<sup>378</sup> A.B.B., S.D. and E.S. are lead authors as they contributed equally to the  
<sup>379</sup> paper and the order of the three names is alphabetical. A.B.B was responsible  
<sup>380</sup> for the Linear AR and Granger causality calculations, and the text describing  
<sup>381</sup> those methods. S.D. was responsible for the GPs used in the paper and was  
<sup>382</sup> responsible for the usage of all the Landsat data and the text describing those  
<sup>383</sup> methods. E.S. was responsible for the MODIS data accumulation, creation of  
<sup>384</sup> the MODIS time series and the filtering of the MODIS data and the text describ-  
<sup>385</sup> ing those methods. SO and PR developed the initial idea and provided feedback  
<sup>386</sup> throughout. All authors wrote, reviewed and edited the final manuscript. We  
<sup>387</sup> acknowledge early contributions to pilot work from Peter Hurley, Philip Rooney,  
<sup>388</sup> Martin Jung, and Jörn Scharlemann.

<sup>389</sup> **Acknowledgements**

<sup>390</sup> This research was funded by the STFC through the following projects: “As-  
<sup>391</sup> troCast: Applying Astronomy Data Analysis to enhance disaster forecasting”  
<sup>392</sup> – grant number ST/R004811/1; and “STFC Official Development Assistance  
<sup>393</sup> (ODA) Institutional Award” attached to the same grant and; ”A UK-Africa  
<sup>394</sup> Data Science Network: Capturing the SKA-Driven Data Transformation” grant  
<sup>395</sup> number ST/R001898/1. This research was also funded by the Science for  
<sup>396</sup> Humanitarian Emergencies and Resilience (SHEAR) consortium project ‘To-  
<sup>397</sup> wards Forecast-based Preparedness Action’ (ForPAC, [www.fopac.org](http://www.fopac.org)), grant  
<sup>398</sup> numbers NE/P000673/1, NE/P000568/1, NE/P000428/1 and NE/P000444/1.  
<sup>399</sup> This project was initiated through pump-priming funding from the University  
<sup>400</sup> of Sussex’s “Sussex Research” thematic programme and carried out as part of

Table A.4: Table comparing Landsat and MODIS products

Feature	Landsat	MODIS
<b>Spatial Resolution</b>	High resolution at 30 m	Medium resolution ranging from 250 m to 1 km
<b>Temporal Resolution</b>	16-day sampling (8-day when both Landsat-7 and 8 are used)	Daily sampling monitoring dynamic variables
<b>Quality</b>	Cloud coverage at 30 m	Cloud coverage at 500 m

401 the interdisciplinary Data Intensive Science Centre at the University of Sussex  
 402 (DISCUS)

#### 403 **Appendix A. Comparison of the two datasets**

404 The key differences between the two datasets are the spatial and temporal  
 405 resolutions, see Table A.4. The Landsat data had higher spatial resolution,  
 406 whilst the MODIS data had higher temporal resolution. Since forecasting was  
 407 being attempted at the level of large scale regions (livelihood zone and county  
 408 intersections), and at a weekly temporal resolution, the expectation was that the  
 409 MODIS data would have advantages, assuming individual Landsat and MODIS  
 410 observations have similar signal-to-noise ratios. The processed MODIS time  
 411 series with weekly observations have less measurement noise because they are  
 412 composites of 7 daily observations ([that themselves are 16-day composites of](#)  
 413 [measurements taken every 1-2 days](#)), whereas the processed Landsat time series  
 414 are derived from more temporally sparse data (up to 3 different Landsat mis-  
 415 sions, each yielding one observation every 16 days). Landsat data would have  
 416 advantages in different applications where forecasts on smaller spatial scales are  
 417 required. The Landsat data also has the advantage that the quality flags and  
 418 cloud masks are defined on smaller scales.

419 The differences between the MODIS and Landsat datasets produced slightly  
 420 different “True” aggregate time series on which to assess the interpolation and  
 421 forecasting methods. In addition to the different temporal resolution of the

422 observations supplying the final time series, the MODIS data were aggregated  
423 across 100 random grassland pixels from each region, whereas the 1 000 Landsat  
424 pixels analysed were randomly distributed over the whole of each region. In  
425 choosing how many pixels to analyse per region, there is a trade-off between  
426 using a larger number of pixels for higher accuracy, and a smaller number of  
427 pixels for lower computational cost. Fewer MODIS pixels were used than Land-  
428 sat pixels since they correspond to larger spatial regions. Both these choices of  
429 number of pixels should be sufficient for high accuracy of results, since for Land-  
430 sat data the  $R^2$ -score comparing the average of all pixels from a region with the  
431 average of 100 or 1 000 random pixels was 0.990 and 0.9993 respectively. The  
432 MODIS grassland classification was not available at Landsat resolution, thus un-  
433 ambiguous classification of the smaller Landsat pixels was not possible. This is  
434 unlikely to have made much difference to pixel selection, given that the pastoral  
435 livelihood zones are mostly grasslands (Fig. 1).

436 **Appendix B. Further details on methods**

437 *Appendix B.1. Gaps in processed MODIS data and forecast*

438 Interpolation of gaps in the raw MODIS time series was not carried out when  
439 the length of the gap was longer than a certain maximum,  $L_{\max}$ . In choosing  
440  $L_{\max}$ , a trade off between quality and quantity of remaining observations had  
441 to be made. The choice  $L_{\max} = 6$  was made, after exploring a range of values  
442 and finding results to be not sensitive to the precise choice within the range  
443 between 4 and 8, see Table B.5. This meant that all interpolated observations  
444 were no more than 3 weeks distant from a real observation, which is within the  
445 range for which interpolation can be assumed to be reasonably accurate, given  
446 the forecasting results found. Note that interpolation on the Landsat data was  
447 carried out for all gaps, since GP the interpolation method makes use of the

Table B.5: Comparison of outcomes for different choices of maximum allowed interpolation length  $L_{\max}$  on the MODIS data. Percentage standard deviation remaining,  $S$ , at 4 weeks, and the percentage of the time that it was possible to make a forecast, for  $L_{\max} = 4, 6$ , and 8. Numbers show the median across all regions.

$L_{\max}$	$S$ at 4 weeks	Forecasts attempted (%)
4	63	84
6	65	93
8	61	98

448 entire time series, and interpolated values within a long interpolation take values  
 449 close to the seasonal mean.

450 Due to the presence of non-interpolated gaps in the MODIS time series, there  
 451 were weeks when a forecast assessment was not carried out on these data. The  
 452 criteria for being able to do AR forecasting on these data were: (i) the three  
 453 most recent weekly aggregated observations had to be present, since these are  
 454 required for making a prediction; (ii) there had to be an aggregated observation  
 455 present for the week being forecast, so the quality of the prediction could be  
 456 assessed.<sup>3</sup>

457 *Appendix B.2. Comparison of other possible gap-filling methods*

458 Various gap-filling methods have been used to deal with missing values re-  
 459 sulting from the presence of clouds and atmospheric aerosols. These methods are  
 460 based on one of three approaches, these include the use of spatial information,  
 461 temporal information within time series and a combination of both spatial  
 462 and temporal (spatio-temporal) information for interpolation(Weiss et al., 2014)  
 463 There is a choice of methods for gap-filling (Kandasamy et al., 2013; Weiss et al.,  
 464 2014), and these fall into the categories of temporal interpolation and spatial in-  
 465 terpolation. Temporal interpolation was chosen given that spatial interpolation  
 466 methods suffer from the fact that there are frequently clouds over Kenya that

---

<sup>3</sup>GP forecasting was still possible when (i) failed, but was also not carried out in that case, since performance would have been worse than usual in this case.

Table B.6: Comparison of GP method with commonly used interpolation methods as candidates for gap-filling on Landsat data. At the pixel level a random observation was removed, and then interpolated with each of the listed methods.

Method	$R^2$ -score
GP	0.67
Linear	0.53
Quadratic	-0.07
Cubic	-1.92
Last value	0.34
Mean value	0.0

467 cover large groups of neighbouring pixels (although a possible alternative, not  
 468 considered here, would be to make use of other pixels that historically behave  
 469 similarly in time (Cao et al., 2018)).

470 The performance of the temporal gap-filling methods employed, compared  
 471 with alternative temporal gap-filling methods, was tested by removing observa-  
 472 tions, applying the method, and then comparing the interpolated observations  
 473 with the removed observations. GP interpolation and linear, quadratic and  
 474 cubic polynomial interpolation methods were tested, on both the Landsat and  
 475 MODIS datasets.  $R^2$ -scores were obtained for using the interpolated values to  
 476 predict the “true” values for the missing observations.

477 For the Landsat data, one randomly chosen observation between 1/1/2014  
 478 and 1/2/2019 was removed from each of 2000 randomly selected individual pixel  
 479 time series.<sup>4</sup> From the MODIS data, 2000 random individual pixel NDVI time  
 480 series (1/1/2014 to 1/2/2019) were chosen. 20 randomly selected NDVI values  
 481 were dropped from each of the time series and the various gap-filling methods  
 482 were used to interpolate the dropped values. The results for Landsat are shown  
 483 in Table B.6 and for MODIS in Table B.7.

---

<sup>4</sup>We remove the mean of the individual NDVI time series for every single observed and interpolated datum before calculating the  $R^2$ -scores. This avoids an over-estimate of the denominator (see Equation 4) due to the variance from different regions in Kenya. This also forces the mean value prediction to be zero, which it should be for a  $R^2$  calculation.

Table B.7: Comparison of interpolation methods as candidates for gap-filling on MODIS data.

Method	$R^2$ -score
GP	0.92
Linear	0.93
Quadratic	0.94
Cubic	0.92
Last value	0.70
Mean value	-0.02

484 For the Landsat data, the GP method achieved the highest  $R^2$ -score, thus  
 485 showing its utility, and justifying our choosing it. The  $R^2$ -score of 0.67, achieved  
 486 by the GP method, is close to the  $R^2$ -score of 0.76 which is obtained from using  
 487 one Landsat observation to predict another Landsat observation of the same  
 488 pixel on the same day (see Section 3). For interpolation the linear method was  
 489 also somewhat effective, achieving an  $R^2$ -score of 0.53.

490 For the MODIS data, GP, linear interpolation and quadratic interpolation  
 491 all performed similarly well. Quadratic interpolation had the highest  $R^2$ -score,  
 492 hence this method was chosen for gap-filling on the MODIS data. The higher in-  
 493 terpolation  $R^2$ -scores for MODIS, compared to Landsat, imply that the MODIS  
 494 data is less noisy than the Landsat data. Assuming that observations from  
 495 MODIS and Landsat have similar signal-to-noise ratio, this can be explained  
 496 by the higher temporal resolution of MODIS, and the compositing of [multiple](#)  
 497 observations for the weekly gridded MODIS data.

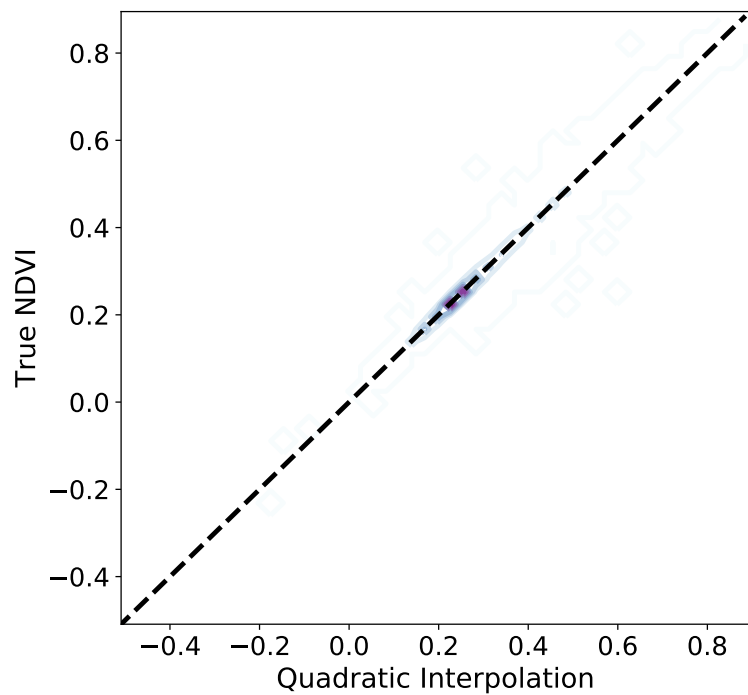


Figure C.8: Contour plot of MODIS observed and predicted NDVI values from 2000 pixels for the Quadratic Interpolation gap-filling

498    **Appendix C. Interpolation**

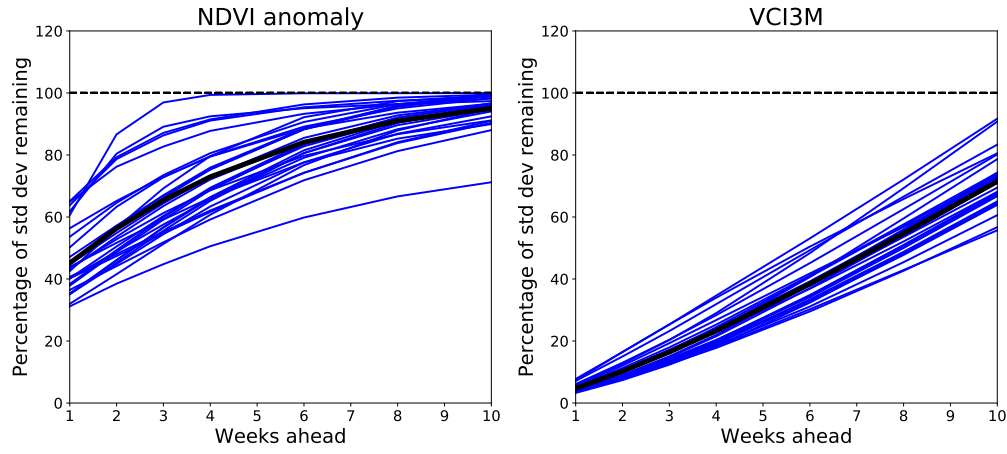


Figure D.9: Forecast performance with a lead time of 1 to 10 weeks using the GP method on the Landsat data, as given by percentage standard deviation remaining  $S$ , for (Left) NDVI anomaly, and (Right) VCI3M. The blue lines show results for the individual regions (county/livelihood zone intersections), and the black line shows the median across all regions.

499 **Appendix D. Forecast**

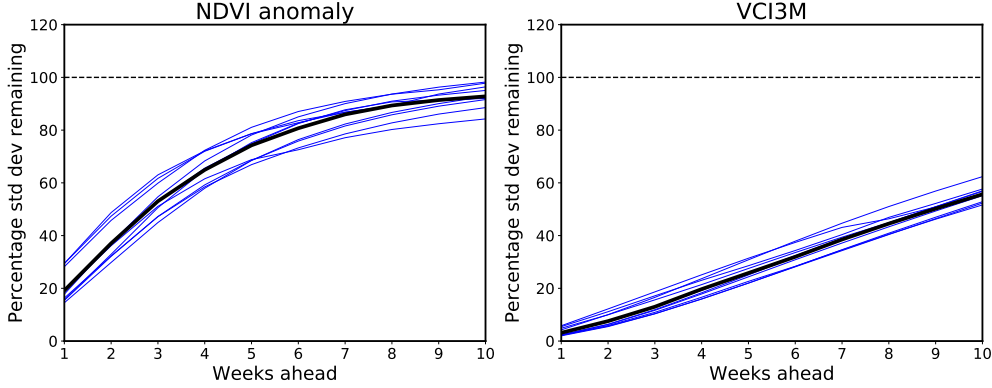


Figure D.10: Forecast performance with a lead time of 1 to 10 weeks using the AR method on the MODIS data, as given by percentage standard deviation remaining, for (Left) NDVI anomaly, and (Right) VCI3M. The blue lines show results for the individual regions for which a forecast is possible more than 50% of the time, and the black line shows the median across all 19 of these regions.

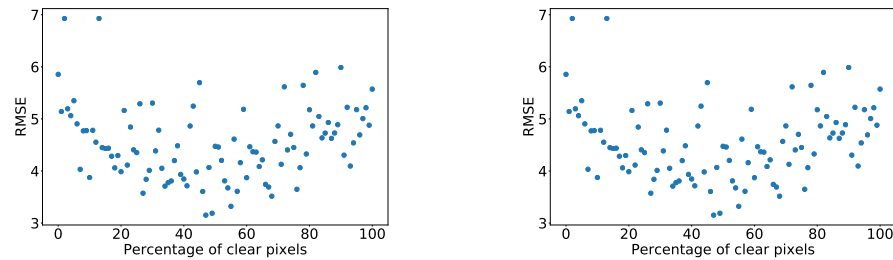


Figure D.11: TO DO: STEVEN/EDWARD REPLACE LEFT HAND PLOTS WITH THE CORRESPONDING PLOTS FROM LANDSAT/GP. ADAM: REFERENCE TO THIS FROM MAIN TEXT. RMSE of 4 week forecast against percentage of clear pixels at most recent observation. (Left) Landsat/GP (Right) MODIS/AR, for which the Pearson correlation is 0.01.

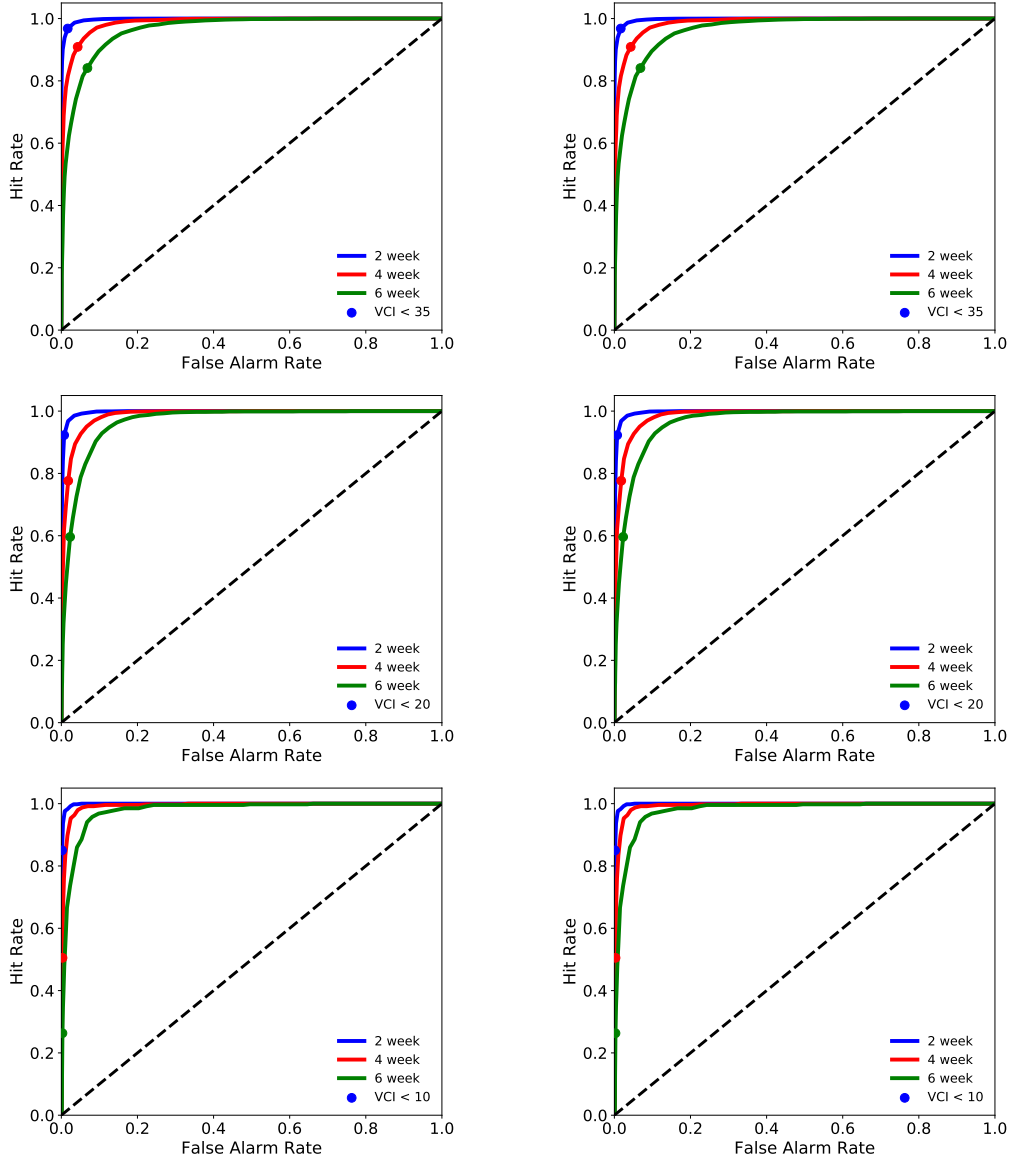


Figure D.12: TO DO: ADAM REPLACE LEFT HAND PLOTS WITH THE CORRESPONDING PLOTS FROM LANDSAT/GP. ROC curves for predicting drought with drought defined at various NDMA thresholds. For (Left) Landsat/GP (Right) MODIS/AR: (Top) Any drought,  $VCI_{3M} < 35$ , (Middle) Severe or extreme drought  $VCI_{3M} < 20$ , (Bottom) Extreme drought  $VCI_{3M} < 10$ .

Table D.8: NDVI anomaly forecast using Landsat data for the 29 regions. The numbers shown are the proportion of standard deviation remaining (Equation 8) and the  $R^2$ -score for NDVI anomaly. We only used past data for the interpolation and we the average value for every pixel within the region for the region estimate. The \* indicates regions where a minimum of 180 detections per pixel were used, instead of 250.

Region	2 weeks	4 weeks	6 weeks
Baringo Z24	46 0.74	66 0.46	81 0.19
Elgeyo-Marakwet Z24	49 0.74	69 0.47	83 0.22
Garissa Z10*	55 0.64	73 0.36	86 0.12
Garissa Z11*	63 0.58	80 0.33	89 0.16
Isiolo Z5	57 0.64	75 0.37	88 0.13
Isiolo Z9	65 0.53	79 0.30	89 0.13
Isiolo Z10	79 0.31	91 0.08	96 -0.02
Isiolo Z24	57 0.67	76 0.41	89 0.19
Kajiado Z15	45 0.76	63 0.52	78 0.28
Kajiado Z18*	44 0.75	59 0.55	72 0.34
Laikipia Z24	42 0.82	61 0.62	77 0.39
Lamu Z11*	80 0.33	92 0.12	95 0.07
Mandera Z7	76 0.25	88 0.00	93 -0.13
Mandera Z9	53 0.44	69 0.06	80 -0.27
Marsabit Z5	52 0.60	66 0.35	78 0.11
Marsabit Z7*	47 0.76	62 0.59	74 0.40
Narok Z15	56 0.67	80 0.34	92 0.12
Narok Z18	56 0.68	75 0.42	88 0.20
Samburu Z5	49 0.68	69 0.36	84 0.08
Samburu Z24	45 0.78	65 0.54	81 0.30
Tana River Z11*	65 0.57	81 0.33	91 0.15
Turkana Z1	54 0.56	72 0.21	84 -0.09
Turkana Z3	38 0.61	51 0.33	60 0.06
Turkana Z24	46 0.75	66 0.48	81 0.21
Wajir Z7*	48 0.71	62 0.51	74 0.30
Wajir Z9	79 0.20	91 -0.07	95 -0.18
Wajir Z10	87 0.24	99 0.01	100 0.00
WestPokot Z1	50 0.69	69 0.43	83 0.18
WestPokot Z24	49 0.68	66 0.42	79 0.16
Median	53 0.67	69 0.36	84 0.15

500    *Appendix D.1. Tables of NDVI and VCI3M forecast*

Table D.9: VCI3M forecast performance using GPs on the Landsat data. The numbers shown are the percentage standard deviation remaining and the  $R^2$  score, respectively.

Region	2 weeks	4 weeks	6 weeks
Baringo Z24	9 0.99	22 0.95	38 0.86
Elgeyo-Marakwet Z24	9 0.99	21 0.96	36 0.87
Garissa Z10	10 0.99	23 0.95	39 0.85
Garissa Z11	11 0.99	25 0.94	41 0.83
Isiolo Z5	10 0.99	23 0.95	39 0.85
Isiolo Z9	11 0.99	24 0.94	38 0.85
Isiolo Z10	13 0.98	29 0.92	46 0.79
Isiolo Z24	10 0.99	23 0.95	39 0.85
Kajiado Z15	9 0.99	21 0.96	36 0.87
Kajiado Z18	9 0.99	20 0.96	34 0.88
Laikipia Z24	7 0.99	18 0.97	32 0.89
Lamu Z11	13 0.98	29 0.92	45 0.80
Mandera Z7	15 0.98	32 0.90	49 0.76
Mandera Z9	12 0.98	29 0.92	48 0.77
Marsabit Z5	11 0.99	25 0.94	41 0.83
Marsabit Z7	8 0.99	19 0.96	32 0.90
Narok Z15	10 0.99	25 0.94	41 0.83
Narok Z18	11 0.99	24 0.94	40 0.84
Samburu Z5	10 0.99	24 0.94	42 0.83
Samburu Z24	8 0.99	20 0.96	35 0.88
TanaRiver Z11	11 0.99	24 0.94	40 0.84
Turkana Z1	14 0.98	31 0.90	52 0.73
Turkana Z3	12 0.99	26 0.93	43 0.81
Turkana Z24	9 0.99	22 0.95	38 0.85
Wajir Z7	9 0.99	20 0.96	34 0.88
Wajir Z9	16 0.97	35 0.88	53 0.72
Wajir Z10	17 0.97	35 0.88	52 0.73
WestPokot Z1	9 0.99	23 0.95	39 0.85
WestPokot Z24	10 0.99	22 0.95	38 0.85
Median	10 0.99	24 0.94	39 0.85

Table D.10: VCI3M forecast performance using AR on the MODIS data. The numbers shown are the percentage standard deviation remaining and the  $R^2$  score, respectively. In the 'Forecasts' column, the number gives the percentage of time points for which it was possible to obtain a forecast.

Region	2 weeks	4 weeks	6 weeks	Forecasts
Baringo Z24	6 0.99	18 0.96	32 0.89	100
Elgeyo-Marakwet Z24	6 0.99	18 0.96	32 0.89	95
Garissa Z10	11 0.98	20 0.95	53 0.71	15
Garissa Z11	xx xx	xx xx	xx xx	0
Isiolo Z5	12 0.98	27 0.92	42 0.81	97
Isiolo Z9	13 0.98	28 0.91	43 0.81	89
Isiolo Z10	13 0.98	28 0.91	42 0.81	71
Isiolo Z24	8 0.99	22 0.95	37 0.86	93
Kajiado Z15	12 0.98	26 0.92	39 0.84	75
Kajiado Z18	11 0.98	24 0.94	38 0.85	71
Laikipia Z24	9 0.99	23 0.94	37 0.85	93
Lamu Z11	xx xx	xx xx	xx xx	0
Mandera Z7	15 0.97	34 0.87	53 0.71	44
Mandera Z9	16 0.97	35 0.87	55 0.69	43
Marsabit Z5	9 0.99	21 0.95	34 0.88	94
Marsabit Z7	17 0.96	35 0.87	48 0.76	34
Narok Z15	11 0.98	28 0.92	44 0.79	96
Narok Z18	6 0.99	19 0.96	32 0.89	98
Samburu Z24	5 0.99	16 0.97	30 0.90	100
Samburu Z5	7 0.99	21 0.95	37 0.86	100
Tana River Z11	11 0.98	22 0.95	33 0.88	41
Turkana Z1	7 0.99	20 0.95	35 0.87	98
Turkana Z3	7 0.99	23 0.94	40 0.83	100
Turkana Z24	7 0.99	20 0.95	35 0.87	100
Wajir Z7	14 0.97	30 0.90	44 0.79	45
Wajir Z9	16 0.97	33 0.88	50 0.74	41
Wajir Z10	12 0.98	23 0.94	33 0.88	19
West Pokot Z1	7 0.99	21 0.95	38 0.85	100
West Pokot Z24	9 0.99	22 0.94	36 0.86	94
Median	11 0.99	23 0.95	38 0.85	93

Table D.11: NDVI anomaly forecast performance using AR on the MODIS data. The numbers shown are the percentage standard deviation remaining and the  $R^2$  score, respectively.

Region	2 weeks	4 weeks	6 weeks
Baringo Z24	32 0.90	59 0.65	75 0.42
Elgeyo-Marakwet Z24	32 0.90	58 0.66	73 0.46
Garissa Z10	42 0.82	51 0.74	56 0.68
Garissa Z11	xx xx	xx xx	xx xx
Isiolo Z5	55 0.69	79 0.37	90 0.18
Isiolo Z9	36 0.87	64 0.58	80 0.35
Isiolo Z10	37 0.86	65 0.57	82 0.32
Isiolo Z24	29 0.91	57 0.66	76 0.42
Kajiado Z15	47 0.78	71 0.48	82 0.31
Kajiado Z18	45 0.79	72 0.48	87 0.24
Laikipia Z24	38 0.85	62 0.60	77 0.40
Lamu Z11	xx xx	xx xx	xx xx
Mandera Z7	33 0.89	64 0.58	87 0.24
Mandera Z9	32 0.89	65 0.57	90 0.18
Marsabit Z5	38 0.85	64 0.59	75 0.44
Marsabit Z7	35 0.88	58 0.66	71 0.49
Narok Z15	48 0.76	72 0.48	83 0.30
Narok Z18	36 0.87	61 0.62	72 0.47
Samburu Z24	28 0.92	56 0.68	73 0.46
Samburu Z5	47 0.78	74 0.45	86 0.25
Tana River Z11	53 0.71	68 0.54	87 0.24
Turkana Z1	32 0.89	64 0.58	82 0.32
Turkana Z3	33 0.89	71 0.49	88 0.21
Turkana Z24	31 0.90	62 0.61	80 0.35
Wajir Z7	29 0.91	54 0.70	67 0.54
Wajir Z9	30 0.91	57 0.67	74 0.44
Wajir Z10	26 0.93	37 0.86	46 0.79
West Pokot Z1	37 0.86	68 0.53	85 0.28
West Pokot Z24	42 0.82	65 0.57	78 0.39
Median	36 0.87	65 0.58	80 0.35

Table D.12: NDVI anomaly forecast performance using GPs on the MODIS data. The numbers shown are the percentage standard deviation remaining and the  $R^2$  score, respectively.

Region	2 weeks	4 weeks	6 weeks
Baringo Z24	37 0.86	73 0.44	93 0.10
Elgeyo-Marakwet Z24	37 0.85	73 0.40	91 0.07
Garissa Z10	46 0.75	59 0.50	68 0.21
Garissa Z11	xx xx	xx xx	xx xx
Isiolo Z5	60 0.60	87 0.16	96 0.02
Isiolo Z9	42 0.83	79 0.38	97 0.08
Isiolo Z10	41 0.82	77 0.36	95 0.05
Isiolo Z24	34 0.89	70 0.51	92 0.15
Kajiado Z15	48 0.75	76 0.35	90 0.09
Kajiado Z18	47 0.78	77 0.40	94 0.11
Laikipia Z24	43 0.81	72 0.46	89 0.16
Lamu Z11	xx xx	xx xx	xx xx
Mandera Z7	39 0.86	74 0.50	97 0.17
Mandera Z9	35 0.89	71 0.54	96 0.20
Marsabit Z5	42 0.79	69 0.37	80 0.11
Marsabit Z7	37 0.80	61 0.38	74 0.09
Narok Z15	50 0.72	76 0.32	87 0.09
Narok Z18	39 0.84	74 0.42	90 0.11
Samburu Z5	50 0.70	80 0.26	91 0.05
Samburu Z24	34 0.88	71 0.48	92 0.12
TanaRiver Z11	60 0.47	75 0.13	87 -0.00
Turkana Z1	36 0.87	75 0.44	95 0.10
Turkana Z3	35 0.88	80 0.37	99 0.03
Turkana Z24	35 0.87	75 0.42	95 0.07
Wajir Z7	31 0.86	57 0.45	72 0.15
Wajir Z9	36 0.85	65 0.45	79 0.15
Wajir Z10	37 0.77	53 0.37	68 -0.17
WestPokot Z1	41 0.83	77 0.39	96 0.08
WestPokot Z24	49 0.78	86 0.34	103 0.06
Median	39 0.83	74 0.40	92 0.09

Table D.13: NDVI anomaly forecast performance using AR on Landsat data. The numbers shown are the percentage standard deviation remaining and the  $R^2$  score, respectively.

Region	2 weeks	4 weeks	6 weeks
Baringo Z24	67 0.54	89 0.19	105 -0.12
Elgeyo-Marakwet Z24	74 0.44	98 0.03	113 -0.28
Garissa Z10	77 0.39	96 0.07	108 -0.17
Garissa Z11	78 0.38	94 0.10	106 -0.13
Isiolo Z5	86 0.25	103 -0.06	114 -0.31
Isiolo Z9	96 0.06	109 -0.20	116 -0.35
Isiolo Z10	108 -0.17	120 -0.46	126 -0.60
Isiolo Z24	66 0.55	82 0.31	92 0.13
Kajiado Z15	59 0.64	78 0.38	91 0.15
Kajiado Z18	60 0.63	76 0.40	90 0.18
Laikipia Z24	54 0.70	75 0.42	93 0.12
Lamu Z11	88 0.20	97 0.05	103 -0.07
Mandera Z7	78 0.38	87 0.23	93 0.12
Mandera Z9	56 0.67	69 0.51	76 0.41
Marsabit Z5	76 0.41	91 0.15	103 -0.07
Marsabit Z7	52 0.72	66 0.55	78 0.38
Narok Z15	79 0.36	101 -0.02	109 -0.19
Narok Z18	73 0.46	91 0.15	101 -0.02
Samburu Z5	74 0.44	95 0.08	110 -0.21
Samburu Z24	60 0.63	81 0.32	97 0.05
TanaRiver Z11	90 0.17	108 -0.18	120 -0.46
Turkana Z1	80 0.35	103 -0.07	118 -0.39
Turkana Z3	75 0.43	95 0.09	111 -0.24
Turkana Z24	69 0.52	91 0.16	106 -0.14
Wajir Z7	53 0.70	63 0.59	70 0.50
Wajir Z9	77 0.40	85 0.27	84 0.27
Wajir Z10	100 0.00	111 -0.24	117 -0.37
WestPokot Z1	70 0.50	92 0.15	107 -0.15
WestPokot Z24	73 0.45	96 0.06	114 -0.31
Median	74 0.44	92 0.15	106 -0.13

501     *Appendix D.2. Assessing forecasting with the inclusion of additional variables*

For the MODIS data, we tested to see whether we could improve the prediction of NDVI anomaly by including the past of other available variables in the AR model, i.e. we performed a Granger causality analysis. Taking  $X$  as NDVI anomaly, as in equation (6), for another variable  $Y$ , the extended model was fit:

$$X_{t+n} = \sum_{i=0}^{p-1} a_i X_{t-i} + \sum_{i=0}^{q-1} b_i Y_{t-i} + \epsilon'_t, \quad (\text{D.1})$$

502     and Granger causality measured as  $\Delta R^2$ , the  $R^2$ -score obtained from this ex-  
503     tended model minus the  $R^2$ -score obtained from the previous (reduced) model  
504     (6).

505     Firstly, we tested whether including past observations of either the red band  
506     or the NIR band (at the same lags as NDVI anomaly) in the regression to  
507     predict NDVI anomaly could improve the quality of the forecast, and found it  
508     did not. For a lead time of 4 weeks, for example, the improvement in  $R^2$ -score  
509     was generally negative; the mean improvement across regions was -0.007 for red  
510     and -0.01 for NIR.

511     Secondly, we tested for Granger causality of NDVI anomaly from each region  
512     to each other region (within the set of regions for which predictions could be  
513     made more than 50% of the time). That is, for each pair of distinct regions,  $i$  and  
514      $j$ , the 3 most recent observations from region  $j$  were added to the AR forecast  
515     model for region  $i$ , and the  $R^2$ -score was compared with that obtained without  
516     including observations from region  $j$ . There was not strong Granger causality of  
517     NDVI anomaly between most regions. For only a few combinations was there an  
518     improvement in  $R^2$ -score of more than 0.05, see Fig. D.13. Nevertheless, these  
519     results suggest that, to create the optimal linear regression based forecasting  
520     method, data from all regions should be used. Future work will explore how  
521     best to extract any useful information from regions other than the one being

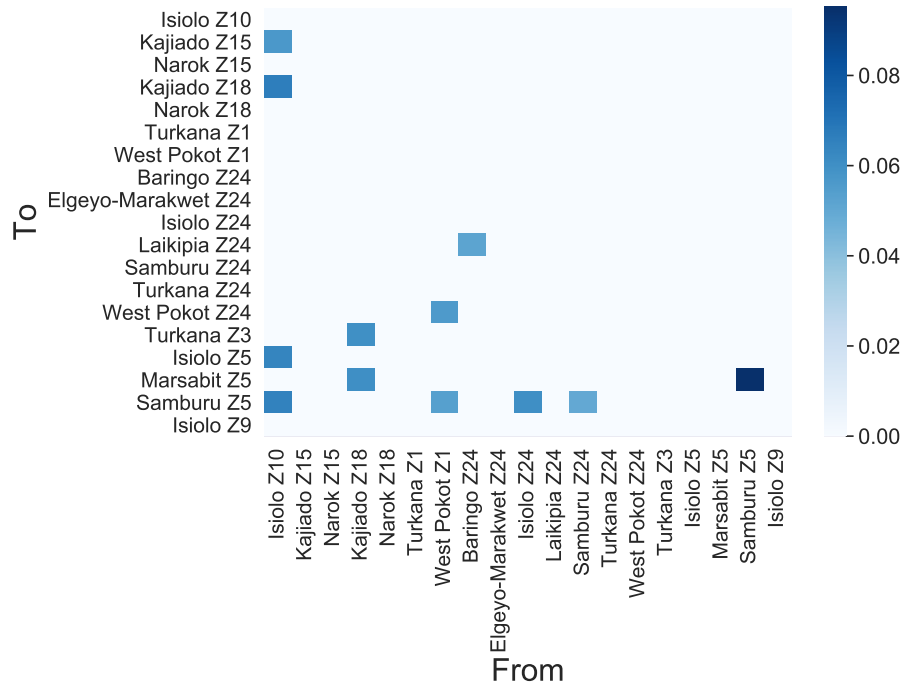


Figure D.13: Granger causality of NDVI anomaly from each region to each other region, computed on the MODIS data, measured as improvement in  $R^2$ -score when observations from region ‘From’ are added to the AR model for forecasting region ‘To’ at a lead time of 4 weeks. Only substantial Granger causalities are shown, i.e. those with  $\Delta R^2 > 0.05$ .

forecast.

523      **References**

- 524      Adede C, Oboko R, Wagacha PW, Atzberger C. A Mixed Model Ap-  
525      proach to Vegetation Condition Prediction Using Artificial Neural Networks  
526      (ANN): Case of Kenya's Operational Drought Monitoring. *Remote Sens-*  
527      ing
- 528      2019;11(9):1099. URL: <https://www.mdpi.com/2072-4292/11/9/1099>.  
528      doi:10.3390/rs11091099.
- 529      AghaKouchak A, Farahmand A, Melton F, Teixeira J, Anderson M, Wardlow  
530      BD, Hain C. Remote sensing of drought: Progress, challenges and opportu-  
531      nities. *Reviews of Geophysics* 2015;53(2):452–80.
- 532      Asoka A, Mishra V. Prediction of vegetation anomalies to improve food  
533      security and water management in india. *Geophysical Research Let-*  
534      *ters* 2015;42(13):5290–8. URL: <https://agupubs.onlinelibrary.wiley.com/doi/abs/10.1002/2015GL063991>.  
535      doi:10.1002/2015GL063991.  
536      arXiv:<https://agupubs.onlinelibrary.wiley.com/doi/pdf/10.1002/2015GL063991>.
- 537      Behnke R, Muthami D. The Contribution of Livestock to the Kenyan  
538      Economy. Technical Report; 2011. URL: [https://cgospace.cgiar.org/bitstream/handle/10568/24972/IGAD{\\_}LPI{\\_}WP{\\_}03-11.pdf?sequence=1&isAllowed=y](https://cgospace.cgiar.org/bitstream/handle/10568/24972/IGAD{_}LPI{_}WP{_}03-11.pdf?sequence=1&isAllowed=y).
- 541      Bhuiyan C, Singh R, Kogan F. Monitoring drought dynamics in the aravalli  
542      region (india) using different indices based on ground and remote sensing  
543      data. *International Journal of Applied Earth Observation and Geoinforma-*  
544      *tion* 2006;8(4):289 – 302. URL: <http://www.sciencedirect.com/science/article/pii/S030324340600016X>. doi:<https://doi.org/10.1016/j.jag.2006.03.002>.
- 547      Brahim-Belhouari S, Vesin JM. Bayesian learning using gaussian process for  
548      time series prediction. In: Proceedings of the 11th IEEE Signal Processing

- 549      Workshop on Statistical Signal Processing (Cat. No.01TH8563). 2001. p. 433–  
550      6. doi:[10.1109/SSP.2001.955315](https://doi.org/10.1109/SSP.2001.955315).
- 551      Brown ME, Kshirsagar V. Weather and international price shocks on food  
552      prices in the developing world. *Global Environmental Change* 2015;35:31  
553      – 40. URL: <http://www.sciencedirect.com/science/article/pii/S0959378015300248>. doi:<https://doi.org/10.1016/j.gloenvcha.2015.08.003>.
- 556      Camps-Valls G, Verrelst J, Munoz-Mari J, Laparra V, Mateo-Jimenez F, Gomez-  
557      Dans J. A survey on gaussian processes for earth-observation data analysis: A  
558      comprehensive investigation. *IEEE Geoscience and Remote Sensing Magazine*  
559      2016;4(2):58–78. doi:[10.1109/MGRS.2015.2510084](https://doi.org/10.1109/MGRS.2015.2510084).
- 560      Cao R, Chen Y, Shen M, Chen J, Zhou J, Wang C, Yang W. A simple method  
561      to improve the quality of ndvi time-series data by integrating spatiotemporal  
562      information with the savitzky-golay filter. *Remote Sensing of Environment*  
563      2018;217:244 –57. URL: <http://www.sciencedirect.com/science/article/pii/S0034425718303985>. doi:<https://doi.org/10.1016/j.rse.2018.08.022>.
- 566      Chandola V, Vatsavai RR. A scalable gaussian process analysis algorithm  
567      for biomass monitoring. *Statistical Analysis and Data Mining: The ASA*  
568      Data Science Journal 2011;4(4):430–45. URL: <https://onlinelibrary.wiley.com/doi/abs/10.1002/sam.10129>. doi:[10.1002/sam.10129](https://doi.org/10.1002/sam.10129). arXiv:<https://onlinelibrary.wiley.com/doi/pdf/10.1002/sam.10129>.
- 571      Chen J, Jönsson P, Tamura M, Gu Z, Matsushita B, Eklundh L. A simple  
572      method for reconstructing a high-quality NDVI time-series data set based on  
573      the Savitzky-Golay filter. *Remote Sensing of Environment* 2004;91(3-4):332–  
574      44. doi:[10.1016/j.rse.2004.03.014](https://doi.org/10.1016/j.rse.2004.03.014).

- 575 Duvenaud D, Lloyd J, Grosse R, Tenenbaum J, Zoubin G. Structure discovery  
576 in nonparametric regression through compositional kernel search. In:  
577 Dasgupta S, McAllester D, editors. Proceedings of the 30th International  
578 Conference on Machine Learning. Atlanta, Georgia, USA: PMLR; volume 28  
579 of *Proceedings of Machine Learning Research*; 2013. p. 1166–74. URL:  
580 <http://proceedings.mlr.press/v28/duvenaud13.html>.
- 581 FAO . Food and Agriculture Organization(FAO) COUNTRY PROGRAMMING  
582 FRAMEWORK FOR KENYA (2014-2017). Technical Report; 2014. URL:  
583 [www.fao.org/publications](http://www.fao.org/publications).
- 584 FEWS-NET . Scenario development for food security early warning. 2018. URL: [https://fews.net/sites/default/files/documents/reports/Guidance\\_Document\\_Scenario\\_Development\\_2018.pdf](https://fews.net/sites/default/files/documents/reports/Guidance_Document_Scenario_Development_2018.pdf).
- 585 Galvin KA, Boone RB, Smith NMS, Lynn SM. Impacts of climate variability  
586 on east african pastoralists: linking social science and remote sensing. 2001. .
- 587 Hamilton J. Time series analysis. Princeton, NJ: Princeton University Press,  
588 1994.
- 589 Kandasamy S, Baret F, Verger A, Neveux P, Weiss M. A comparison  
590 of methods for smoothing and gap filling time series of remote sensing  
591 observations – application to modis lai products. Biogeosciences  
592 2013;10(6):4055–71. URL: <https://www.biogeosciences.net/10/4055/2013/>. doi:10.5194/bg-10-4055-2013.
- 593 Kim JJ, Guha-Sapir D. Famines in africa: is early warning early  
594 enough? Global Health Action 2012;5(1):18481. URL: <https://doi.org/10.3402/gha.v5i0.18481>.  
595 arXiv:<https://doi.org/10.3402/gha.v5i0.18481>.

- 600 Klisch A, Atzberger C. Operational drought monitoring in kenya using modis  
601 ndvi time series. *Remote Sensing* 2016;8(4). URL: <http://www.mdpi.com/2072-4292/8/4/267>. doi:10.3390/rs8040267.
- 603 Kogan F. Application of vegetation index and brightness temperature  
604 for drought detection. *Advances in Space Research* 1995;15(11):91 –  
605 100. URL: <http://www.sciencedirect.com/science/article/pii/027311779500079T>. doi:[https://doi.org/10.1016/0273-1177\(95\)00079-T](https://doi.org/10.1016/0273-1177(95)00079-T); *natural Hazards: Monitoring and Assessment Using Remote Sensing Technique*.
- 609 Kogan F, Adamenko T, Guo W. Global and regional drought dynamics in the  
610 climate warming era. *Remote Sensing Letters* 2013;4(4):364–72. URL: <https://doi.org/10.1080/2150704X.2012.736033>. doi:10.1080/2150704X.2012.736033. arXiv:<https://doi.org/10.1080/2150704X.2012.736033>.
- 613 Lesk C, Rowhani P, Ramankutty N. Influence of extreme weather disasters on  
614 global crop production. *Nature* 2016;529:84 EP –. URL: <https://doi.org/10.1038/nature16467>.
- 616 Mishra AK, Singh VP. A review of drought concepts. *Journal of Hydrology*  
617 2010;391(1):202 –16. URL: <http://www.sciencedirect.com/science/article/pii/S0022169410004257>. doi:<https://doi.org/10.1016/j.jhydrol.2010.07.012>.
- 620 Nelson GC, Valin H, Sands RD, Havlík P, Ahammad H, Deryng D, El-  
621 liott J, Fujimori S, Hasegawa T, Heyhoe E, Kyle P, Von Lampe  
622 M, Lotze-Campen H, Mason d'Croz D, van Meijl H, van der Mens-  
623 brugghe D, Müller C, Popp A, Robertson R, Robinson S, Schmid E,  
624 Schmitz C, Tabeau A, Willenbockel D. Climate change effects on agri-  
625 culture: Economic responses to biophysical shocks. *Proceedings of*

- 626 the National Academy of Sciences 2014;111(9):3274–9. URL: <https://www.pnas.org/content/111/9/3274>. doi:10.1073/pnas.1222465110.  
627 arXiv:<https://www.pnas.org/content/111/9/3274.full.pdf>.
- 629 Nyong A, Adesina F, Osman Elasha B. The value of indigenous knowledge  
630 in climate change mitigation and adaptation strategies in the african sa-  
631 hel. Mitigation and Adaptation Strategies for Global Change 2007;12(5):787–  
632 97. URL: <https://doi.org/10.1007/s11027-007-9099-0>. doi:10.1007/  
633 s11027-007-9099-0.
- 634 Orindi V, Nyong A, Herrero MT. Pastoral livelihood adaptation to drought and  
635 institutional interventions in kenya 2007;.
- 636 Papagiannopoulou C, Gonzalez Miralles D, Decubber S, Demuzere M, Ver-  
637 hoest N, Dorigo WA, Waegeman W. A non-linear granger-causality frame-  
638 work to investigate climate-vegetation dynamics. GEOSCIENTIFIC MODEL  
639 DEVELOPMENT 2017;10(5):1945–60. URL: <http://dx.doi.org/10.5194/gmd-10-1945-2017>.
- 641 Coughlan de Perez E, van den Hurk B, van Aalst MK, Jongman B,  
642 Klose T, Suarez P. Forecast-based financing: an approach for cat-  
643 alyzing humanitarian action based on extreme weather and climate fore-  
644 casts. Natural Hazards and Earth System Sciences 2015;15(4):895–  
645 904. URL: <https://www.nat-hazards-earth-syst-sci.net/15/895/2015/>. doi:10.5194/nhess-15-895-2015.
- 647 Piguet E, Pécoud A, de Guchteneire P. Migration and Climate Change:  
648 An Overview. Refugee Survey Quarterly 2011;30(3):1–23. URL:  
649 <https://doi.org/10.1093/rsq/hdr006>. doi:10.1093/rsq/hdr006.  
650 arXiv:<http://oup.prod.sis.lan/rsq/article-pdf/30/3/1/4460951/hdr006.pdf>.

- 651 Tozier de la Poterie A, Baudoin MA. From yokohama to sendai: Approaches  
652 to participation in international disaster risk reduction frameworks. International  
653 Journal of Disaster Risk Science 2015;6(2):128–39. URL: <https://doi.org/10.1007/s13753-015-0053-6>.
- 655 Rasmussen CE, Williams CKI. Gaussian processes for machine learning 2006;;
- 656 Rojas O, Vrieling A, Rembold F. Assessing drought probability for agri-  
657 cultural areas in africa with coarse resolution remote sensing imagery.  
658 Remote Sensing of Environment 2011;115(2):343 –52. URL: <http://www.sciencedirect.com/science/article/pii/S0034425710002798>.  
659 doi:<https://doi.org/10.1016/j.rse.2010.09.006>.
- 661 Roy D, Wulder M, Loveland T, Woodcock C, Allen R, Anderson M, Helder D,  
662 Irons J, Johnson D, Kennedy R, Scambos T, Schaaf C, Schott J, Sheng Y, Ver-  
663 mote E, Belward A, Bindschadler R, Wohen W, Gao F, Zhu Z. Landsat-8: Sci-  
664 ence and product vision for terrestrial global change research. Remote Sensing  
665 of Environment 2014;2014:154–72. doi:[10.1016/j.rse.2014.02.001](https://doi.org/10.1016/j.rse.2014.02.001).
- 666 Rulinda CM, Bijker W, Stein A. The chlorophyll variability in meteosat derived  
667 ndvi in a context of drought monitoring. Procedia Environmental Sciences  
668 2011;3:32 –7. URL: <http://www.sciencedirect.com/science/article/pii/S1878029611000089>. doi:<https://doi.org/10.1016/j.proenv.2011.02.007>; 1st Conference on Spatial Statistics 2011 – Mapping Global Change.
- 671 Sai F, Cumiskey L, Weerts A, Bhattacharya B, Haque Khan R. To-  
672 wards impact-based flood forecasting and warning in bangladesh: a  
673 case study at the local level in sirajganj district. Natural Hazards  
674 and Earth System Sciences Discussions 2018;2018:1–20. URL: <https://www.nat-hazards-earth-syst-sci-discuss.net/nhess-2018-26/>.  
675 doi:[10.5194/nhess-2018-26](https://doi.org/10.5194/nhess-2018-26).

- 677 Savitzky A, Golay MJE. Smoothing and Differentiation of Data by Sim-  
678 plified Least Squares Procedures. Analytical Chemistry 1964;36(8):1627–  
679 39. URL: <http://pubs.acs.org/doi/abs/10.1021/ac60214a047>. doi:10.  
680 1021/ac60214a047.
- 681 Schaaf C, Wang Z. MCD43A4 MODIS/Terra+Aqua BRDF/Albedo  
682 Nadir BRDF Adjusted Ref Daily L3 Global - 500m V006 [Data  
683 set]. 2015. URL: [https://lpdaac.usgs.gov/dataset{\\_}discovery/modis/modis{\\_}products{\\_}table/mcd43a4{\\_}v006](https://lpdaac.usgs.gov/dataset{_}discovery/modis/modis{_}products{_}table/mcd43a4{_}v006). doi:10.5067/MODIS/MCD43A4.006.
- 686 Stanke C, Kerac M, Prudhomme C, Medlock J, Murray V. Health effects of  
687 drought: a systematic review of the evidence. PLoS currents 2013;5. URL:  
688 <https://www.ncbi.nlm.nih.gov/pubmed/23787891>.
- 689 Stocker TF, Qin D, Plattner GK, Tignor M, Allen SK, Boschung J, Nauels A,  
690 Xia Y, Bex V, Midgley PM, et al. Climate change 2013: The physical science  
691 basis. 2013.
- 692 Tierney JE, Ummenhofer CC, deMenocal PB. Past and future rainfall in  
693 the horn of africa. Science Advances 2015;1(9). URL: <https://advances.sciencemag.org/content/1/9/e1500682>. doi:10.1126/sciadv.1500682.  
694 arXiv:<https://advances.sciencemag.org/content/1/9/e1500682.full.pdf>.
- 696 UNDP . KENYA – ADAPTATION TO CLIMATE CHANGE IN ARID LANDS  
697 (KACCAL) - KENYA CASE STUDY. Technical Report; 2013. URL: <http://gefonline.org/projectDetailsSQL.cfm?projID=3792>.
- 699 Upadhyay D, Huang W, Kong W, Pascucci S, Pignatti S, Zhou X, Ye H, Casa  
700 R. A comparison of hybrid machine learning algorithms for the retrieval of  
701 wheat biophysical variables from sentinel-2. Remote Sensing 2019;11(5). URL:  
702 <http://www.mdpi.com/2072-4292/11/5/481>. doi:10.3390/rs11050481.

- 703 Venton CC, Fitzgibbon C, Shitarek T, Coulter L, Dooley O. The economics of  
704 early response and disaster resilience: lessons from kenya and ethiopia. Final  
705 report 2012;.
- 706 Vrieling A, Meroni M, Mude AG, Chantarat S, Ummenhofer CC, de Bie  
707 KC. Early assessment of seasonal forage availability for mitigating the im-  
708 pact of drought on east african pastoralists. *Remote Sensing of Environ-*  
709 *ment* 2016;174:44 – 55. URL: <http://www.sciencedirect.com/science/article/pii/S0034425715302248>. doi:<https://doi.org/10.1016/j.rse.2015.12.003>.
- 710
- 711
- 712 Weiss DJ, Atkinson PM, Bhatt S, Mappin B, Hay SI, Gething PW. An  
713 effective approach for gap-filling continental scale remotely sensed time-  
714 series. *ISPRS Journal of Photogrammetry and Remote Sensing* 2014;98:106–  
715 18. URL: <https://www.sciencedirect.com/science/article/pii/S0924271614002512>. doi:[10.1016/J.ISPRSJPRS.2014.10.001](https://doi.org/10.1016/J.ISPRSJPRS.2014.10.001).
- 716
- 717 WMO . Wmo guidelines on multi-hazard impact-based forecast and warning  
718 services 2015;.
- 719
- 720 Yang H, Huntingford C. Brief communication. drought likelihood for east africa.  
Natural Hazards and Earth System Sciences 2018;18(2):491–7.
- 721
- 722 Zambrano F, Vrieling A, Nelson A, Meroni M, Tadesse T. Prediction of drought-  
723 induced reduction of agricultural productivity in chile from modis, rain-  
724 fall estimates, and climate oscillation indices. *Remote Sensing of Environ-*  
725 *ment* 2018;219:15 – 30. URL: <http://www.sciencedirect.com/science/article/pii/S0034425718304541>. doi:<https://doi.org/10.1016/j.rse.2018.10.006>.
- 726
- 727 Zargar A, Sadiq R, Naser B, Khan FI. A review of drought indices. *Environ-*  
728 *mental Reviews* 2011;19(NA):333–49.

<sup>729</sup> Zhang L, Jiao W, Zhang H, Huang C, Tong Q. Studying drought  
<sup>730</sup> phenomena in the continental united states in 2011 and 2012 using  
<sup>731</sup> various drought indices. Remote Sensing of Environment 2017;190:96  
<sup>732</sup> – 106. URL: <http://www.sciencedirect.com/science/article/pii/S0034425716304813>. doi:<https://doi.org/10.1016/j.rse.2016.12.010>.